



**DISSIPATION, DISPERSION AND STABILITY OF
NUMERICAL SCHEMES FOR ADVECTION
AND DIFFUSION**

by Pierre Schoeffler

| | | |
|---|-------------------------|---------------------|
| Issuing Agency SMHI Box 923 S-601 19 NORRKÖPING SWEDEN | Report number RMK 34 | |
| Report date July 1983 | | |
| Author(s) | | |
| Pierre Schoeffler | | |
| Title (and Subtitle) Dissipation, dispersion and stability properties of numerical schemes for advection and diffusion | | |
| <p>Abstract</p> <p>Advection and diffusion are fundamental processes in the atmosphere. They express the permanent balance between inertial and viscous forces. Some numerical treatments the equations, describing these processes, are presented. Three spatial discretization techniques, second order finite differences, linear finite element and pseudo-spectral, are tested in connection with a finite difference time integration. Dissipation, dispersion and stability of the numerical schemes for the linearized equations are investigated both theoretically and with the help of numerical simulations. Results with non-linear equations are also shown.</p> <p>In conclusion there is a presentation of the less conventional Monte Carlo method for diffusion.</p> | | |
| Key words Numerical methods, advection, diffusion, linear finite elements, pseudo-spectral, Monte Carlo | | |
| Supplementary notes | Number of pages 55 | Language English |
| ISSN and title 0347-2116 SMHI Reports Meteorology and Climatology | | |
| Report available from: Liber Grafiska AB/Förlagsorder S-162 89 STOCKHOLM SWEDEN | | |

L I S T O F C O N T E N T

| | Page |
|---|------|
| 1. METHODS OF DISCRETIZATION OF PARTIAL DIFFERENTIAL EQUATION | 1 |
| 1.1 <u>Finite differences</u> | 1 |
| 1.2 <u>Finite elements</u> | 1 |
| 1.3 <u>Pseudo-spectral</u> | 3 |
| 2. METHODS FOR INVESTIGATING LINEAR STABILITY AND ACCURACY OF NUMERICAL SCHEMES | 5 |
| 2.1 <u>Taylor development</u> | 5 |
| 2.2 <u>Fourier development or von Neumann's method</u> | 5 |
| 3. NUMERICAL SCHEMES FOR ADVECTION | 8 |
| 3.1 <u>Linear theory</u> | 8 |
| 3.2 <u>Numerical experiments</u> | 10 |
| 4. NUMERICAL SCHEMES FOR DIFFUSION | 15 |
| 4.1 <u>Linear theory</u> | 15 |
| 4.2 <u>Numerical experiment</u> | 17 |
| 5. A STATISTICAL APPROACH TO THE DIFFUSION EQUATION | 18 |
| 6. FILTERING TECHNIQUE | 22 |
| 7. CONCLUSION - OPTIMAL CHOICE OF A METHOD | 23 |

DEFINITIONS

aliasing

in non-linear theory; misrepresentation by the grid of a not \rightarrow^1 resolvable wave. Its apparition is due to a non-linear interaction between two waves whose wavenumber lies near the limit of the \rightarrow resolvability of the grid

aliasing error

in non-linear theory; the error due to an \rightarrow aliasing

computational phase speed
or diffusion coefficient

in linear theory; the coefficient needed to keep the advective or diffusive expression of the equation when the \rightarrow elementary solution is substituted into the numerical scheme

conservation

a numerical scheme is conservative in regards to a physical invariant of the equation if the numerical expression of this invariant is conserved by the approximated equation

consistency

a numerical scheme is consistent if the approximation of derivatives approaches the derivative when the grid interval approaches zero

convergence

a numerical scheme is convergent if the error approaches zero when the grid interval approaches zero for any initial conditions.
Remark: \rightarrow consistency does not guarantee convergence.

dispersion

in linear theory; a numerical scheme is dispersive if the \rightarrow computational phase speed or diffusion coefficient is a function of the wave number of the \rightarrow elementary solution

dissipation

the inverse of \rightarrow conservation

elementary solution

in linear theory, a wave solution of the advection or diffusion equation

error

the error of the numerical solution is the difference between the numerical and the true solution

linear stability

stability of the numerical scheme approximating the linearized equation

order of accuracy

lowest power of the grid interval that appears in the \rightarrow truncation error

non-linear instability

in non-linear theory; instability due to the spurious energy flow associated by the \rightarrow aliasing error

resolvability

property inherent to a discrete grid which expresses its ability to resolve wavelengths longer than two grid intervals (limit of resolvability)

¹ word also found in this list

DEFINITIONS, continuation

| | |
|------------------|---|
| stability | a numerical scheme is stable if the error remains bounded as the time increases for any initial conditions |
| truncation error | additional term needed to keep the equations valid when the true solution is substituted into the numerical scheme and developed in Taylor series |

1. METHODS OF DISCRETIZATION OF PARTIAL DIFFERENTIAL EQUATIONS

Three types of space discretization are considered.

1.1 Finite differences

The derivatives are approximated by finite difference quotients: difference between values of the variable at grid points over the grid interval, with the requirement that the approximation is consistent. Generally, the conditions of stability are then necessary and sufficient to ensure convergence (Arakawa, 1976).

The time derivatives are approximated by this method in the following study.

1.2 Finite elements

The variable is expanded by using a discrete series of piecewisely defined polynomial functions, called the basis functions.

Let us consider the one-dimensional problem

$$\frac{\partial \phi}{\partial t} + L\phi = 0 \quad \text{for } x \leq \Omega = [x_1, x_M] \quad (1)$$

where L is a spatial differential operator.

To each point x_m of the grid is associated a basis function $\alpha_m(x)$

$$\alpha_m(x_n) = \delta_{m,n} \quad \begin{cases} =1 & \text{if } m = n \\ =0 & \text{if } m \neq n \end{cases} \quad (2)$$

An approximation of $\phi(x,t)$ is:

$$\tilde{\phi}(x,t) = \sum_{n=1}^M \phi_n(t) \alpha_n(x)$$

with $\phi_n(t) = \phi(x_n, t)$

The procedure of discretization of the equation consists of substituting the approximated solution into the equation and orthogonalizing the residual to the basis functions (Galerkin procedure):

$$\int_{\Omega} (\frac{\partial \tilde{\phi}}{\partial t} - L\tilde{\phi}) \alpha_n dx = 0 \quad n=1, \dots M \quad (3)$$

After time discretization, it remains to solve a system of M equations for M unknowns.

If L is a linear operator, one gets:

$$\sum_{m=1}^M \frac{d\phi_m}{dt} \int_{\Omega} \alpha_m \alpha_n dx = \sum_{m=1}^M \phi_m \int_{\Omega} \alpha_n L\alpha_m dx \quad n=1, \dots M$$

The method has two characteristics (Cullen, 1979):

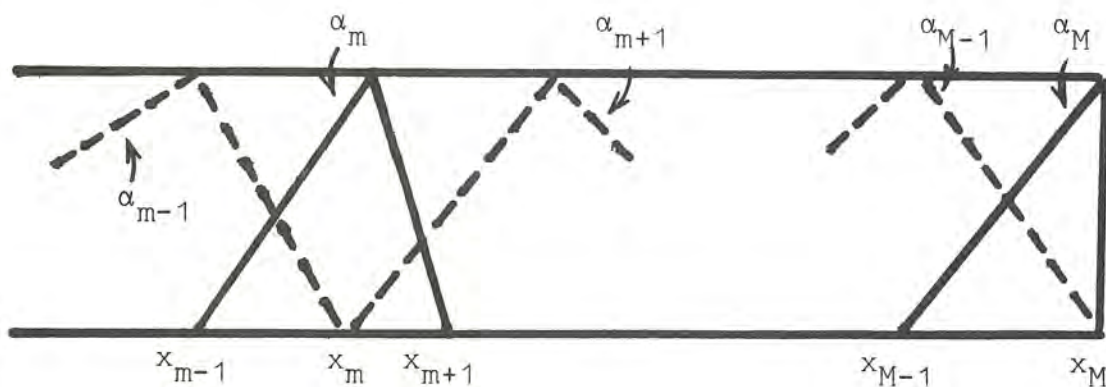
- the piecewise definition of the basis functions implies an almost orthogonality to one another (local interaction). This gives rise to a local spatial coupling between time derivatives (term $\int_{\Omega} \alpha_n \alpha_m dx$). The method is, by essence, an implicit method which needs the inversion of a sparse matrix each time step. The advantage consists of an improved description of the computational phase speed or diffusion coefficient and, in some case, of an increased order of accuracy (super convergence).
- The Galerkin integral guarantees aliasing free and conservative schemes. The effect of this integral is to prevent the appearance of a solution not resolvable by the basis function polynomial space. As the spectral method, the finite element method can be introduced as a least square approximation.

In all its generality, a finite element is the combination of

- a polynomial function space
- a set of points
- a geometric form

defined in such a way that the relation (2) permits a one-to-one relation between points and basis functions.

The simplest one-dimensional finite element is constituted by a linear polynomial defined on a segment:



The great flexibility of the method is due to the large freedom in the definition of the geometric form. Small elements can be concentrated where much information is desired, curved triangular or rectangular elements can be used to integrate with great precision the geometry of the boundaries (Johnson, 1980).

1.3 Pseudo-spectral method

The space derivatives at the grid points are calculated in wave number space. The variable ϕ is expanded by using a discrete series of globally defined trigonometric functions.

$$\phi(x,t) = \sum_k A(k,t) e^{ikx} \quad (4)$$

The amplitudes $A(k,t)$ are computed by the inverse relation of (4). The derivatives are then:

$$\frac{\partial \phi}{\partial x} = \sum_k i k A(k,t) e^{ikx}$$

$$\frac{\partial^2 \phi}{\partial x^2} = \sum_k (-k^2) A(k,t) e^{ikx}$$

etc ...

The method has two characteristics (Merilees and Orszag, 1979).

- this evaluation of space derivatives may be considered as equivalent to the use of a certain finite differences scheme involving all the grid points, the weights of which are decreasing when the distance from the point under consideration increases.

For an infinitely differentiable variable, that leads to an infinite order of accuracy and, in reverse, to the problem of the remote influence of small perturbations.

- The calculation of the space derivatives in the spectral space makes the scheme essentially explicit. The stability conditions are furthermore restricted by the increasing space accuracy (of, for example, the stability condition for Leap Frog in Table I). It must be noticed that periodic boundary conditions and a regular grid are needed to apply the method.

If $M = 2N+1$, considerations of periodicity and resolvability give the resolvable wave numbers:

$$k_j = \frac{2\pi}{(2N+1)\Delta x} j \quad -N \leq j \leq N \quad \Delta x \text{ is the grid interval}$$

The transformation physical spectral space and its inverse are:

$$\phi(x_m, t) = \sum_{j=-N}^{+N} A(k_j, t) e^{i k_j x_m}, \quad 1 \leq m \leq 2N+1 \quad (4)$$

$$A(k_j, t) = \frac{1}{2N+1} \sum_{m=1}^{2N+1} \phi(x_m, t) e^{-i k_j x_m}, \quad -N \leq j \leq N \quad (5)$$

2. METHODS FOR INVESTIGATING LINEAR STABILITY AND ACCURACY OF NUMERICAL SCHEMES

2.1 Taylor development

The true solution is substituted into the numerical scheme and developed in Taylor series. The truncation error gives then the order of accuracy and, in some cases, the stability condition.

2.2 Fourier development or von Neumann's method

This method permits a systematic investigation of stability conditions and a study of the accuracy by examining the behaviour of the computational phase speed or diffusion coefficient.

Advection:

Let us consider

$$\boxed{\frac{\partial \phi}{\partial t} + c \frac{\partial \phi}{\partial x} = 0} \quad (6)$$

c is the physical phase speed, constant in time.

An elementary solution of (6) is

$$\phi(x,t) = \exp(-i k c t) \exp(i k x) \quad (7)$$

k is the wave number.

After time and space discretization,

$$\begin{aligned} \phi(m\Delta x, l\Delta t) &= \phi_m^l = \exp(-i k v l \Delta t) \exp(i k m \Delta x) \\ &= g^l \exp(i k m \Delta x) \end{aligned} \quad (8)$$

v is the computational phase speed, g is the amplification factor

$$g = |g| \exp(i\theta) = \exp(-i k v \cdot \Delta t) \quad (9)$$

The introduction of the expression (8) into the numerical scheme under consideration gives g as a function of c, Δt and Δx .

The stability criterion is obtained by

$$\boxed{|g(c, \Delta t, \Delta x)| \leq 1} \quad (10)$$

The behaviour of v in non-dimensional form is obtained from (9):

$$\boxed{\frac{v}{c} = -\frac{\theta}{R k \Delta x} + i \frac{\log|g|}{R k \Delta x}} \quad (11)$$

where $R = \frac{c \Delta t}{\Delta x}$

Remark. $k \Delta x$ varies from II (the least resolvable wave length is $2\Delta x$) to 0 (wave degenerated into a constant)

Diffusion:

Let us consider

$$\boxed{\frac{\partial \phi}{\partial t} = \frac{\partial}{\partial z} K \frac{\partial \phi}{\partial z} = K \frac{\partial^2 \phi}{\partial z^2} + \frac{dK}{dz} \frac{\partial \phi}{\partial z}} \quad (12)$$

K is the physical diffusion coefficient, constant in time.

An elementary solution of (12) is

$$\phi(x, t) = \exp \left[\left(i k \frac{dK}{dz} - k^2 K \right) t \right] \exp (i k z) \quad (13)$$

After time and space descretization,

$$\begin{aligned} \phi(m\Delta z, l\Delta t) &= \phi_m^l = \exp \left[\left(i k \frac{d\rho}{dz} - k^2 \rho \right) l\Delta t \right] \exp (i k m\Delta z) \\ &= g^l \exp (i k m\Delta z) \end{aligned} \quad (14)$$

ρ is the computational diffusion coefficient

g is the amplification factor

$$g = |g| \exp (i\theta) = \exp \left[\left(i k \frac{d\rho}{dz} - k^2 \rho \right) \Delta t \right] \quad (15)$$

The introduction of the expression (14) into the numerical scheme under consideration gives g as a function of K , $\frac{dK}{dz}$, Δt , Δz .

The stability criterion is obtained by

$$\boxed{|g(K, \frac{dK}{dz}, \Delta t, \Delta z)| \leq 1} \quad (16)$$

The behaviour of ρ and $\frac{d\rho}{dz}$ in non-dimensional form is obtained from (15):

$$\frac{\rho}{K} = - \frac{1}{S(k\Delta z)^2} \log |g| \quad (17)$$

$$\frac{d\rho}{dz}/\frac{dK}{dz} = \frac{\theta}{T(k\Delta z)} \quad (18)$$

where $S = \frac{K\Delta t}{\Delta z^2}$, $T = \frac{dK}{dz} \frac{\Delta t}{\Delta z}$

3. NUMERICAL SCHEMES FOR ADVECTION

Only the most widely used schemes are discussed here.

3.1 Linear theory

Table I recapitulates name, expression, order of accuracy, amplification factor and stability condition for all wave numbers of each scheme.

The symbol in parenthesis refers to the tables II, a through h, where the ratio v/c is presented depending on R and $k\Delta x$ following (11).

Relation (11) shows that $|g| < 1$ produces a complex computational phase speed which is a source of dissipation (only the real values are exhibited in table II).

Table II shows that all schemes, whose expression is not strictly symmetric in time and space are dissipative. Only Leap-Frog and Crank-Nicholson escape. The amount of damping is quite large for shorter wave lengths, especially for the wave length $2\Delta x$. A disadvantage lies in the fact that damping also depends, for a fixed Δx , on the time step Δt and the advection velocity c . However, we wish to choose Δt to give the best accuracy and stability properties, not to give the optimal amount of damping.

The Lax-Wendroff scheme is symmetric but a diffusion term is added in order to dissipate the shorter waves. The scheme can be rewritten explicitly as:

$$\frac{\psi_m^{l+1} - \psi_m^l}{\Delta t} + c \frac{\psi_m^{l+1} - \psi_m^{l-1}}{2\Delta x} = \frac{c^2 \Delta t}{2} \frac{\psi_{m+1}^l - 2\psi_m^l + \psi_{m-1}^l}{\Delta x^2}$$

The effect of introducing a dissipation in a Crank-Nicholson scheme by taking a backward time integration introduces very little change in the real part of the computational phase speed (compare IIb with IIc).

The amplification factor of a three-time-step scheme has two solutions. One gives the computational phase speed of the physical solution, the other one generates a spurious numerical solution, computational mode, whose amplitude changes sign every time-step (only the physical values are exhibited in Tables II). Nevertheless, for the same second order of accuracy, the computational phase speed of the physical solution is better described by a Leap-Frog scheme than by a Crank-Nicholson scheme (compare IIb with IIe).

The linear finite element technique is superior to the finite difference methods for all time integration schemes (compare IIb with IIIf for Crank-Nicholson, IIe with IIg for Leap-Frog). The introduction of an increased order of spatial accuracy is paid for by a restriction on the stability condition for the Leap-Frog scheme: the upper boundary is 1 for a second order finite difference scheme, $1/\sqrt{3}$ for a linear finite element scheme, which is of fourth order and $1/\pi$ for a pseudo-spectral scheme of infinite order of accuracy. Another disadvantage is the large negative computational group speed at short wave lengths. The physical group speed c_g , which represents the velocity of transport of energy, is equal to the phase velocity for a constant phase speed according to the definition: (Holton, 1979, pp 151-152):

$$c_g = \frac{d(ck)}{dk} = c$$

The computational group speed is

$$v_g = \frac{d(vk)}{dk}$$

which is not equal to c because of the dispersive character of the numerical schemes under consideration, e.g. the fact that $v_g = v_g(k)$.

Looking at tables IIb and IIIf, for example, the phase speed of wave-lengths lengths $2\Delta x$ is zero, so the group speed can be approximated by:

$$v_g = \frac{d(vk\Delta x)}{d(k\Delta x)} \approx -v \quad (k\Delta x = \pi/2)$$

The energy propagates upstream in both cases but faster for the finite element scheme (IIIf) than for the finite differences one (IIb). The improved computational phase speed at short wavelengths causes a deteriorated computational group speed.

It may be noticed that the pseudo-spectral scheme does not seem to be superior to the finite element one and that the computational phase speed exceeds for all R and $k\Delta x$ the physical one.

3.2 Numerical experiments

One-dimensional linear advection:

A Gaussian form given by

$$\phi(x, o) = 100 \exp\left(-\frac{(x-x_o)^2}{2}\right)$$

is advected on a 30 discretization points regular grid. The numerical solution is compared with the analytic one, $\phi(x, t) = \phi(x-ct, o)$.

Outflow boundary

Only the finite differences, up-stream and the finite element schemes have a prognostic equation for the boundary value ϕ_M .

For example: the linear finite element leap frog scheme

$$\frac{1}{3} \left(\frac{\phi_{M-1}^{l+1} - \phi_{M-1}^{l-1}}{2\Delta t} + 2 \frac{\phi_M^{l+1} - \phi_M^{l-1}}{2\Delta t} \right) + c \frac{\phi_M^l - \phi_{M-1}^l}{\Delta x} = 0$$

The other finite difference schemes need an additional condition like the no flux condition, $\frac{\partial \phi}{\partial x} = 0$, at the boundary. A special stability analysis must be performed to avoid spurious oscillations near the boundary.

With a pseudo-spectral technique, presupposing cyclic boundary values, the form advected out at the out-flow boundary is reintroduced at the in-flow boundary. To avoid this, Christensen and Prahm (1976) sacrifices the information on a few gridpoints near the out-flow boundary by artificially damping the solution.

In this case equation (6) becomes:

$$\frac{\partial \phi}{\partial t} + c \frac{\partial \phi}{\partial x} + \frac{\phi}{\tau} = 0$$

$\tau = \frac{\Delta x}{c}$ is the e-folding time of the damping

The comparison is made after advection through 12, 16 and 20 (out-flow boundary) gridpoints with $R = 0.25, 0.50$ and 0.75 . Figs Ia, b, c, d, e, f, g and h show the result for the corresponding numerical schemes.

It may be noticed:

- the intensive computational dissipation for asymmetric schemes, in space, the up-stream (Ia), in time Laasonen (Ic) and for the symmetric but intentionally dissipative Lax-Wendroff scheme (Id),

- the considerable reduction of noise in connection with the finite element technique (compare Ib with If for Crank-Nicholson and Ie with Ig for Leap-Frog).

Uniform rotation of a conical distribution

The analytical function describing the cone is given by

$$\phi(x, y, \circ) = \begin{cases} 100 \cos(\pi \frac{d}{2r}) & \text{if } d \leq r \\ 0 & \text{otherwise} \end{cases}$$

with $d^2 = (x - x_0)^2 + (y - y_0)^2$, (x_0, y_0) is the center of the cone
 r is the base radius of the cone

The uniform circular velocity field, centered at (x_1, y_1) (center of the grid) is given by: $\omega(-x + x_1, y - y_1)$, ω is the angular velocity. The grid has 30×30 discretization points separated by a constant interval Δs .

Fig IIa shows the evolution of the numerical solution of the rotation at an angle of 90° , 180° , 270° and 360° for $\omega \Delta t = 0.5^\circ$ and $r = 4\Delta s$.

Fig IIb shows the corresponding evolution of

- the maximal amplitude $\max_{m,n} (\phi_{m,n}^\ell)$, where $\phi_{m,n} = \phi(m\Delta s, n\Delta s, \ell\Delta t)$

$$\frac{\sum_{m,n} \phi_{m,n}^\ell}{\sum_{m,n} \phi_{m,n}^o}$$

- the sum of amplitudes

$$\frac{\sum_{m,n} (\phi_{m,n}^\ell)^2}{\sum_{m,n} (\phi_{m,n}^o)^2}$$

- the sum of amplitudes squares

The evolution of the two first quantities tests the conservative properties of the scheme under consideration, the evolution of the third tests the stability (an unstable scheme can conserve the sum of amplitudes).

Five schemes are tested:

- finite differences/up-stream forward (Ia)
- finite differences/Crank-Nicholson (Ib)
- finite differences/Lax-Wendroff (Id)
- linear finite element/Crank-Nicholson (If)
- pseudo-spectral/Leap-Frog (Ih)

The results call for some comments:

- the up-stream scheme dissipates the maximal amplitude, the sum of amplitudes and the sum of amplitudes squares. Moreover the conical form expands itself with time,
- the finite differences/Lax-Wendroff and Crank-Nicholson show a tendency for a similar behaviour concerning the maximal amplitude and the conical form.
- the finite element/Crank-Nicholson and pseudo-spectral/Leap-Frog conserve exactly the sum of amplitudes and of amplitudes squares and nearly exactly the maximal amplitude and the form of the cone.

The computational times necessary to integrate the two-dimensional linear advection equation under consideration on a SAAB-UNIVAC 1100/21 computer with each of the five schemes are compared below:

the up-stream method acts as standard measure:

| | |
|--|-----|
| finite differences/up-stream forward (Ia) | 1. |
| finite differences/Lax-Wendroff (Id) | 1.4 |
| finite differences/Crank-Nicholson (Ib) | 3.5 |
| linear finite element/Crank-Nicholson (If) | 6.3 |
| pseudo-spectral/Leap-Frog (Ih) | 12. |

The pseudo-spectral technique uses a FORTRAN Fast Fourier Transform elaborated by P. N. Swartzrauber at the NCAR (1978).

One-dimensional non-linear advection

The Burger equation:

$$\frac{\partial \phi}{\partial t} + \phi \frac{\partial \phi}{\partial x} = K \frac{\partial^2 \phi}{\partial x^2} \quad K \text{ constant}$$

together with the following initial condition:

$$\phi(x,0) = \frac{1}{2} (1 - \operatorname{th} \frac{x}{4K})$$

has the analytic solution (Gazdag, 1973):

$$\phi(x,t) = \frac{1}{2} [1 - \operatorname{th} (\frac{x-t/2}{4K})]$$

The true solution is compared with the computational one calculated on a 256 discretization points regular grid by means of the following schemes (for the diffusion schemes, see chapter 4)

- finite differences/up-stream forward

$$\frac{\phi_m^{l+1} - \phi_m^l}{\Delta t} + p \phi_m^l \frac{\phi_m^l - \phi_{m-p}^l}{\Delta x} = K \frac{\phi_{m+1}^{l+1} - 2\phi_m^{l+1} + \phi_{m-1}^{l+1}}{\Delta x^2}$$

$$\text{where } p = \begin{cases} +1 & \text{if } \phi_m^l > 0 \\ -1 & \text{if } \phi_m^l < 0 \end{cases}$$

- finite element/Laasonen

$$\begin{aligned} \frac{\phi_{m-1}^{l+1} - \phi_{m-1}^l}{\Delta t} + 4 \frac{\phi_m^{l+1} - \phi_m^l}{\Delta t} + \frac{\phi_{m+1}^{l+1} - \phi_m^l}{\Delta t} + \\ + \frac{1}{\Delta x} \left[(2\phi_m^l + \phi_{m+1}^l) \phi_{m+1}^{l+1} - (\phi_{m+1}^l - \phi_{m-1}^l) \phi_m^{l+1} - (2\phi_m^l + \phi_{m-1}^l) \phi_{m-1}^{l+1} \right] = \\ = K \frac{\phi_{m+1}^{l+1} - 2\phi_m^{l+1} + \phi_{m-1}^{l+1}}{\Delta x^2} \end{aligned}$$

- pseudo-spectral/Adams-Bashforth

$$\frac{\phi_m^{l+1} - \phi_m^l}{\Delta t} + \phi_m^l \left(\frac{3}{2} \frac{\partial \phi_m^l}{\partial x} - \frac{1}{2} \frac{\partial \phi_m^{l-1}}{\partial x} \right) = K \left(\frac{3}{2} \frac{\partial^2 \phi_m^l}{\partial x^2} - \frac{1}{2} \frac{\partial^2 \phi_m^{l-1}}{\partial x^2} \right)$$

In order to satisfy to the cyclic boundary conditions, the domain of integration D is divided into two subdomains

$$\begin{cases} D_0 \text{ where } \phi \text{ is kept constant} \\ D_1 \text{ where the time integration is realized} \end{cases}$$

The numerical parameters are

$$\Delta x = 0.01, \Delta t = 0.001$$

$$D = [0., 2.55]$$

$$\text{in } D_0 = [0., 0.6], \quad \phi(x) = \begin{cases} 0 & 0 \leq x \leq 0.1 \\ 1 - \cos \frac{(x-0.1)\pi}{0.3} & 0.1 \leq x \leq 0.4 \\ 1 & 0.4 < x < 0.6 \end{cases}$$

$$\text{in } D_1 = 0.6, 2.55, \quad \phi(x, 0) = \frac{1}{2} (1 - \tanh \frac{x-1}{4K})$$

Fig III presents the computed and true profiles between $x = 1.20$ and $x = 1.60$ after 166 time-steps and for $K = 0.002, 0.005$ and 0.01 .

Table III exhibits the values in the transition domain between $x = 1.37$ and $x = 1.49$.

Finite element and pseudo-spectral techniques give nearly same result in good agreement with the true solution, while the finite differences technique both smoothes and retards exaggeratedly the computational solution.

4. NUMERICAL SCHEMES FOR DIFFUSION

Long (1975) has examined 8 different second order finite difference schemes for the diffusion equation. As for the advection only the most widely used schemes are presented here:

4.1 Linear theory

Table IV recapitulates name, expression, order of accuracy, amplification factor and stability conditions for all wave numbers of each scheme. The symbol in parenthesis refers to the table where the ratios ρ/K and $\frac{d\rho}{dz}/\frac{dK}{dz}$ are presented depending on s , T and $k\Delta z$ following (17), (18).

The decomposition of the diffusion into a K - and a $\frac{dK}{dz}$ -term is used for convenience. By this way the behaviour of ρ and $\frac{d\rho}{dz}$ can be examined separately.

The conventional form is obtained considering:

$$K = \frac{K_{m+1/2} + K_{m-1/2}}{2} \text{ and } \frac{dK}{dz} = \frac{K_{m+1/2} - K_{m-1/2}}{\Delta z}$$

For example, IVa becomes (see definition in table on next page)

$$\frac{\phi_m^{\ell+1} - \phi_m^\ell}{\Delta t} = \frac{1}{\Delta z^2} (K_{m+1/2} \phi_{m+1}^\ell - (K_{m+1/2} + K_{m-1/2}) \phi_m^\ell + K_{m-1/2} \phi_{m-1}^\ell)$$

If $\frac{dK}{dz} = 0$, relations (17), (18) become

$$\frac{\rho}{K} = - \frac{1}{s(k\Delta z)^2} \log |g| - i \frac{\theta}{s(k\Delta z)^2}$$

where g is real

and $\theta = \begin{cases} 0 & \text{if } 0 < g \leq 1 \\ \pi & \text{if } -1 \leq g < 0 \end{cases}$

Remark:

$\theta = \pi$ gives rise to a spurious $2\Delta t$ wave (cf (15)).

The condition on s to avoid the appearance of such a wave is:

| numerical scheme | condition of positivity for g |
|--|---------------------------------|
| finite differences forward (IVa) | $4s \leq 1$ |
| finite differences trapezoidal (IVb) | $3s \leq 1$ |
| finite differences (IVc) | $2s \leq 1$ |
| finite differences Crank-Nicholson (IVd) | $2s \leq 1$ |
| finite differences Laasonen (IVe) | $-\nabla s$ |
| finite differences Dufort-Frankel (IVf) | $1 \leq 2s$ |
| linear finite element Laasonen (IVg) | $-\nabla s$ |
| pseudo-spectral Adams-Bashforth (IVh) | $s = 0$ |

Only the Laasonen method guarantees the absence of a $2\Delta t$ noise in the case of weak gradient of diffusion coefficient.

The adoption of a three-time-step scheme as Dufort-Frankel or Adams-Bashforth introduce two solutions: a physical one and a computational one (only the physical values are exhibited in table IV). Fortunately, the ratio ρ/K for the numerical solution goes to infinity when the wavelength increases. The computational mode is thus quickly damped.

Crank-Nicholson (IVd) is apparently better than Dufort-Frankel (IVf). The latter overestimates the shear $\frac{d\rho}{dz}$ at large s .

When T ($= \frac{dK}{dz} \cdot \frac{\Delta t}{\Delta z}$) increases, both ρ and $\frac{d\rho}{dz}$ decrease and underestimate K and $\frac{dK}{dz}$ for all schemes but for Laasonen. This one keeps the ratio ρ/K near one at least for large s (IVe).

The use of finite element in combination with the Laasonen time integration scheme improves the results at small s but amplifies the error at large S , that becomes troublesome at large T (compare IVe with IVg).

4.2 Numerical experiments

One-dimensional linear diffusion with constant coefficient

One considers the linear diffusion of an instantaneous point source

$$\phi(z,0) = 100 \delta(z_0)$$

where $\delta(z_0)$ is the Dirac function $\delta(z_0) = \begin{cases} 1 & z = z_0 \\ 0 & \text{otherwise} \end{cases}$

Considering $\frac{dk}{dz} = 0$ the solution of (12) is for the boundary conditions:
 $\frac{\partial\phi}{\partial z} = 0$ at infinity

$$\phi(z,t) = \frac{100}{\sqrt{4\pi Kt}} \exp \left[-\frac{(z-z_0)^2}{4Kt} \right]$$

The solution computed on a 30 discretization points regular grid with the help of the different schemes is compared with the Gaussian analytical solution after 3, 6 and 12 iterations with $S = 0.25, 0.50$ and 0.75 . Figs IVa, b, c, d, e, f, g and h present the result for the corresponding numerical schemes.

It may be noticed:

- the presence of a spurious $2\Delta z$ wave at some value of S for all the schemes except IVc, which is rather bad, and Laasonen IVe and IVg. This feature is particularly remarkable for Dufort-Frankel, IVf.
- the nearly equivalent description given by the finite element and the finite difference technique (compare IVe with IVg),
- the nearly similar results obtained with Crank-Nicholson, Laasonen and Dufort-Frankel for a weak gradient of diffusion coefficient ($T = 0.25$) and the superiority of the two-time-steps schemes Crank-Nicholson and Laasonen for strong gradient of diffusion coefficient ($T = 0.75$) (compare IVd, IVe and IVf).
- the unstable pseudo-spectral Adams-Basforth scheme at $s = 0.25$ can be rendered stable by filtering the $2\Delta z$ wave, i.e. setting the amplitude of this wave equal to zero in the frequency space.

5. A STATISTICAL APPROACH TO THE DIFFUSION EQUATION

The previous chapter discussed diffusion from an Eulerian point of view, establishing the diffusion equation from a consideration of 'concentration' and flux at fixed points in space.

It is also possible to approach the diffusion problem from a Lagrangian point of view, focusing on the history of random movements executed by the diffusing particles. To get useful results, statistical properties of the random motions have to be considered.

A statistical treatment of the Brownian motion is performed by Csanady (1973). His approach can be generalized in the following way.

Let us consider the velocity field $\mu(t)$ of a diffusing particle (the space coordinates are omitted for simplicity).

Provided the physical process is stationary, it is convenient to define a time autocorrelation coefficient $r(\tau)$, and a Lagrangian integral scale I_L related to r by:

$$I_L = \int_0^\infty r(\tau) d\tau$$

The value of I_L is thus a rough measure of the time interval over which $\mu(t)$ is correlated with itself.

The conventional diffusion coefficient is related to the integral scale by (Tennekes and Lumley, 1972, p 225)

$$K = I_E \sigma^2$$

where σ^2 is the variance of the velocity field $\mu(t)$ and subscript E means an Eulerian property.

In the atmosphere turbulent surface boundary layer:

$$K = l_E \mu_*$$

where l_E is the mixing-length or size of the most energetic turbulent eddies

$\mu_* = \sigma$ is the friction velocity

From dimensional consideration one also has $I_E = \frac{l}{\mu_*}$

For e g $\ell = 5$ m, $\mu_* = 0.25$ m/s, one gets $I_E = 20$ s.

It is reasonable to expect that all the integral scales associated with $\mu(t)$ are about the same, because they are determinated by the scale of the physical processes that produces $\mu(t)$. I is also a measure of the time over which $\mu(t)$ is dependent on itself (Tennekes and Lumley, 1972).

It is thus possible to divide the total displacement of a particle into a number of (nearly) independent random steps, taking place over a time period Δt much larger than I : the particle is said to execute a 'random walk'.

The diffusion of a passive admixture is simulated by tracking a number of N particles, each representing a certain quantity Q . The motion of each particle of number i in one dimension z is described by the following equation:

$$z_i^{\ell+1} = z_i^\ell + \Delta t w^\ell + \Delta t p_i^\ell$$

where z^ℓ holds for $z(\ell\Delta t)$

w is the advection velocity in the z -direction

$\{p^\ell\}$ is a discrete random process, i e a sequence of mutually independent, identically distributed random variables

The transport due to diffusion is further related to the process $\{p^\ell\}$ by introduction of a scale of diffusion velocity P :

$$p_i^\ell = P v_i^\ell$$

where $\{v_i^\ell\}$ are random numbers between -1 and +1 chosen independently from a prescribed probability density function.

For a constant diffusion coefficient K , the diffusion velocity scale P is

$$P = \left(\frac{6K}{\Delta t} \right)^{1/2} \quad (19)$$

But generally, the choice of P is entirely due to convenience.

The mean concentration ψ after a time t_o in a segment of length Δz around z_o is interpreted as the probability for a particle to be in the volume Δz around z_o at time t_o , i.e.:

$$\psi(z_o, t_o) = \frac{Q}{\Delta z} \sum_{i=1}^N \delta_i^{\Delta z}$$

where

$$\delta_i^{\Delta z} = \begin{cases} 1 & \text{if } z_o - \frac{\Delta z}{2} < z_i(t_o) \leq z_o + \frac{\Delta z}{2} \\ 0 & \text{otherwise} \end{cases}$$

The method described above is unconditionally stable, the only limitation lies in the choice of the time step $\Delta t \gg I$ and in the fact that the process has to be stationary.

A numerical experiment analogue to this described in 4.2 is performed: one considers N particles of coordinate $\{z_i\}$, the evolution of which is given by:

$$z_i^{l+1} = z_i^l + \Delta t P v_i^l \quad \text{initially } z_i^0 = z_o \quad \forall i$$

P is related to $s = \frac{K \Delta t}{\Delta z^2}$ using (19):

$$P \Delta t = \Delta z (6s)^{1/2}$$

$$\text{and } \psi_m^l = \frac{100}{N \Delta z} \sum_{i=1}^N \delta_i^{\Delta z}$$

where

$$\delta_i^{\Delta z} = \begin{cases} 1 & (m - \frac{1}{2}) \Delta z \leq z_i^l \leq (m + \frac{1}{2}) \Delta z \\ 0 & \text{otherwise} \end{cases}$$

As before, the statistical solution is compared to the true solution after 3, 6 and 12 iterations in fig. V.

Δz is taken equal to 1.

The numbers $\{v_i^l\}$ are chosen independently from a rectangular probability density function and the number N is chosen as the minimal number of particles which gives an error of the statistical solution less than 10% in regard to the true solution after 12 iterations.

A systematic study shows that, on the mean:

for $S = 0.25$ $N = 120$

$S = 0.50$ $N = 60$

$S = 0.75$ $N = 30$

6. FILTERING TECHNIQUE

The numerical experiments with the advection and diffusion equations show the necessity of filtering spurious short waves, generally two time-step or space-interval waves.

The most usual filter is the so called Asselin filter (1972): if $\tilde{\psi}$ is the smoothed field, ψ the initial field, then

$$\tilde{\psi}_p = \psi_p + \frac{v}{2} (\psi_{p+1} - 2\psi_p + \psi_{p-1})$$

v is the coefficient of the filter

p is a space or time gridpoint index

Table IVa gives the ratio $\tilde{\psi}/\psi$ depending on v and the wavelength (Δs is the grid interval).

A filter much more efficient to damp the shorter waves while keeping unchanged the longer waves is used by Long et alii (1966):

$$(1-v)\tilde{\psi}_{p-1} + 2(1-v)\tilde{\psi}_p + (1-v)\tilde{\psi}_{p+1} = \psi_{p-1} + 2\psi_p + \psi_{p+1}$$

Table IVb indicates its performance. The method is time-consuming because of its implicit character.

As the pseudo-spectral method is concerned, the filtering is reduced to a setting of the amplitudes of the spurious waves to zero in the frequency space.

A selectively controlled filtering has, in all cases, a beneficial effect on the linear and non-linear stability.

7. CONCLUSION - OPTIMAL CHOICE OF A METHOD

To integrate a convection equation, several subjective factors guide the choice of a numerical scheme:

- a computational dissipation is desired or, on the contrary, good conservation properties are looked for.
- The boundary conditions require special attention.
- Precision is more important than computational integration time.

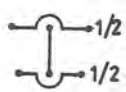
Some other factors have a more imperative character like:

- for the desired grid interval and time step, the stability condition must be fulfilled in regards to the advection velocity, the diffusion coefficient and its derivative,
- a compatibility must exist between the advection and the diffusion schemes as well as for the time integration scheme (two-or-three-time steps) in terms of accuracy in time and space.

Undoubtedly, the linear finite element/Crank-Nicholson scheme presents many good properties for modelling the advection equation: accuracy, conservation, unconditional linear and non-linear stability, good treatment of the boundaries, little dispersion of the computational phase speed. If desired, a controlled dissipation can be added by the introduction of a filter.

For modelling the diffusion equation, the finite differences technique seems to be superior in accuracy to the finite element one, as long as boundary conditions are out of consideration. The problem of non-linear instability which could justify an aliasing free method is not relevant in a diffusion problem where the shorter waves are filtered by the physical process itself as they appear. Some schemes, however, create and maintain a two-grid-interval noise. In this case, an additional selective filter must be used. Finally the finite differences/Laasonen scheme seems to be superior to the others: no spurious, two-grid-interval noise, unconditional linear stability and good accuracy speak in its favour.

Table 1

Comput.
model

24



| Comput. model | Name and expression | Order of accuracy | Amplification factor | Stability condition |
|---------------|--|--------------------------|---|---------------------|
| | finite differences up-stream forward or Euler (Ia) $\frac{\psi_m^{l+1} - \psi_m^l}{\Delta t} + c \cdot \frac{\psi_m^l - \psi_{m-1}^l}{\Delta x} = 0 \text{ for } c > 0$ | $\Delta x, \Delta t$ | $g = 1 + R(\cos k\Delta x - 1) - iR \sin k\Delta x$ | $ R \leq 1$ |
| | finite differences Crank-Nicholson (Ib) $\frac{\psi_m^{l+1} - \psi_m^l}{\Delta t} + \frac{c}{2} \left(\frac{\psi_{m-1}^{l+1} - \psi_{m-1}^l}{2\Delta x} + \frac{\psi_{m-1}^l - \psi_{m-1}^l}{2\Delta x} \right) = 0$ | $\Delta x^2, \Delta t^2$ | $g = \frac{1 - i \frac{R}{2} \sin k\Delta x}{1 + i \frac{R}{2} \sin k\Delta x}$ | $\forall R$ |
| | finite differences Crank-Nicholson backward or Laasonen (Ic) $\frac{\psi_m^{l+1} - \psi_m^l}{\Delta t} + c \frac{\psi_{m+1}^{l+1} - \psi_{m-1}^{l+1}}{2\Delta x} = 0$ | $\Delta x^2, \Delta t$ | $g = \frac{1}{1 + iR \sin k\Delta x}$ | $\forall R$ |
| | finite differences Lax-Wendroff (Id) (Gadd, 1974) $\frac{\psi_{m+1/2}^l - \frac{1}{2}(\psi_{m+1}^l + \psi_m^l)}{\frac{1}{2}\Delta t} + c \frac{\psi_{m+1}^l - \psi_m^l}{\Delta x} = 0$ $\frac{\psi_{m-1/2}^{l+1/2} - \frac{1}{2}(\psi_m^l + \psi_{m-1}^l)}{\frac{1}{2}\Delta t} + c \frac{\psi_m^l - \psi_{m-1}^l}{\Delta x} = 0$ $\frac{\psi_m^{l+1} - \psi_m^l}{\Delta t} + c \frac{\psi_{m+1/2}^{l+1/2} - \psi_{m-1/2}^{l+1/2}}{\Delta x} = 0$ | $\Delta x^2, \Delta t^2$ | $g = 1 + R^2(\cos k\Delta x - 1) - iR \sin k\Delta x$ | $ R \leq 1$ |

Table 1, continuation

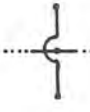
| Comput. model | Name and expression | Order of accuracy | Amplification factor | Stability condition |
|---|---|-------------------------------|--|-------------------------------|
|  | finite differences leap-frog (Ie) $\frac{\psi_m^{l+1} - \psi_m^{l-1}}{2\Delta t} + c \frac{\psi_{m-1}^l - \psi_{m+1}^l}{2\Delta x} = 0$ | $\Delta x^2, \Delta t^2$ | $g = \pm(1 - R^2 \sin^2 k\Delta x)^{1/2} - iR \sin k\Delta x$ | $ R \leq 1$ |
|  | linear finite element Crank-Nicholson (If) $\frac{1}{6} \left(\frac{\psi_{m-1}^{l+1} - \psi_{m-1}^l}{\Delta t} + 4 \frac{\psi_m^{l+1} - \psi_m^l}{\Delta t} + \frac{\psi_{m+1}^{l+1} - \psi_{m+1}^l}{\Delta t} \right) + \\ + \frac{c}{2} \left(\frac{\psi_{m+1}^{l+1} - \psi_{m-1}^{l+1}}{2\Delta x} + \frac{\psi_{m+1}^l - \psi_{m-1}^l}{2\Delta x} \right) = 0$ | $\Delta x^4, \Delta t^2$ | $g = \frac{\frac{2 + \cos k\Delta z}{3} - i \frac{R}{2} \sin k\Delta z}{\frac{2 + \cos k\Delta z}{3} + i \frac{R}{2} \sin k\Delta z}$ | $\forall R$ |
|  | linear finite element leap-frog (Ig) $\frac{1}{6} \left(\frac{\psi_{m-1}^{l+1} - \psi_{m-1}^{l-1}}{2\Delta t} + 4 \frac{\psi_m^{l+1} - \psi_m^{l-1}}{2\Delta t} + \frac{\psi_{m+1}^{l+1} - \psi_{m+1}^{l-1}}{2\Delta t} \right) + \\ + c \frac{\psi_{m+1}^l - \psi_{m-1}^l}{2\Delta x} = 0$ | $\Delta x^4, \Delta t^2$ | $g = \frac{\pm \sqrt{\left[\frac{(2 + \cos k\Delta x)^2 - R^2 \sin^2 k\Delta x}{3} \right]^{1/2} - iR \sin k\Delta x}}{\frac{2 + \cos k\Delta x}{3}}$ | $ R \leq \frac{1}{\sqrt{3}}$ |
|  | pseudo-spectral leap-frog (Ih) $\frac{\psi_m^{l+1} - \psi_m^{l-1}}{2\Delta t} + c \frac{\partial \psi_m}{\partial x} = 0$ | $\Delta x^\infty, \Delta t^2$ | $g = \pm(1 - R^2(k\Delta x)^2)^{1/2} - iR(k\Delta x)$ | $ R < \frac{1}{\pi}$ |

Table IIa - finite differences up-stream forward

| wave length $k\Delta x$ | $2\Delta x$ π | $4\Delta x$ $\pi/2$ | $6\Delta x$ $\pi/3$ | $8\Delta x$ $\pi/4$ |
|----------------------------|----------------------|------------------------|------------------------|------------------------|
| R = 0.25 | 0. | 0.819 | 0.927 | 0.960 |
| R = 0.50 | 0. | 1. | 1. | 1. |
| R = 0.75 | 0. | 1.060 | 1.024 | 1.013 |

Table IIb - finite differences Crank-Nicholson

| | | | | |
|----------|----|-------|-------|-------|
| R = 0.25 | 0. | 0.633 | 0.824 | 0.898 |
| R = 0.50 | 0. | 0.624 | 0.814 | 0.891 |
| R = 0.75 | 0. | 0.609 | 0.800 | 0.880 |

Table IIc - finite differences Laasonen

| | | | | |
|----------|----|-------|-------|-------|
| R = 0.25 | 0. | 0.624 | 0.814 | 0.891 |
| R = 0.50 | 0. | 0.590 | 0.780 | 0.865 |
| R = 0.75 | 0. | 0.546 | 0.733 | 0.828 |

Table IID - finite differences Lax-Wendroff

| | | | | |
|----------|----|-------|-------|-------|
| R = 0.24 | 0. | 0.664 | 0.840 | 0.907 |
| R = 0.50 | 0. | 0.749 | 0.878 | 0.928 |
| R = 0.75 | 0. | 0.865 | 0.936 | 0.960 |

Table IIe - finite differences leap-frog

| | | | | |
|----------|----|-------|-------|-------|
| R = 0.15 | 0. | 0.643 | 0.834 | 0.905 |
| R = 0.50 | 0. | 0.667 | 0.866 | 0.923 |
| R = 0.75 | 0. | 0.720 | 0.900 | 0.949 |

Table IIf - linear finite element Crank-Nicholson

| | | | | |
|----------|----|-------|-------|-------|
| R = 0.25 | 0. | 0.944 | 0.987 | 0.995 |
| R = 0.50 | 0. | 0.914 | 0.971 | 0.985 |
| R = 0.75 | 0. | 0.870 | 0.946 | 0.970 |

Table IIg - linear finite element leap frog

| | | | | |
|----------|----|-------|-------|-------|
| R = 0.25 | 0. | 0.979 | 1.004 | 1.004 |
| R = 0.50 | 0. | 1.080 | 1.044 | 1.025 |
| R = 0.75 | 0. | / | 1.138 | 1.067 |

Table IIh - pseudo-spectral leap frog

| | | | | |
|----------|-------|-------|-------|-------|
| R = 0.25 | 1.150 | 1.028 | 1.012 | 1.007 |
| R = 0.50 | / | 1.150 | 1.052 | 1.028 |
| R = 0.75 | / | / | 1.150 | 1.069 |

$\frac{v}{c}$ / unstable

Figure 1a Finite differences up-stream forward

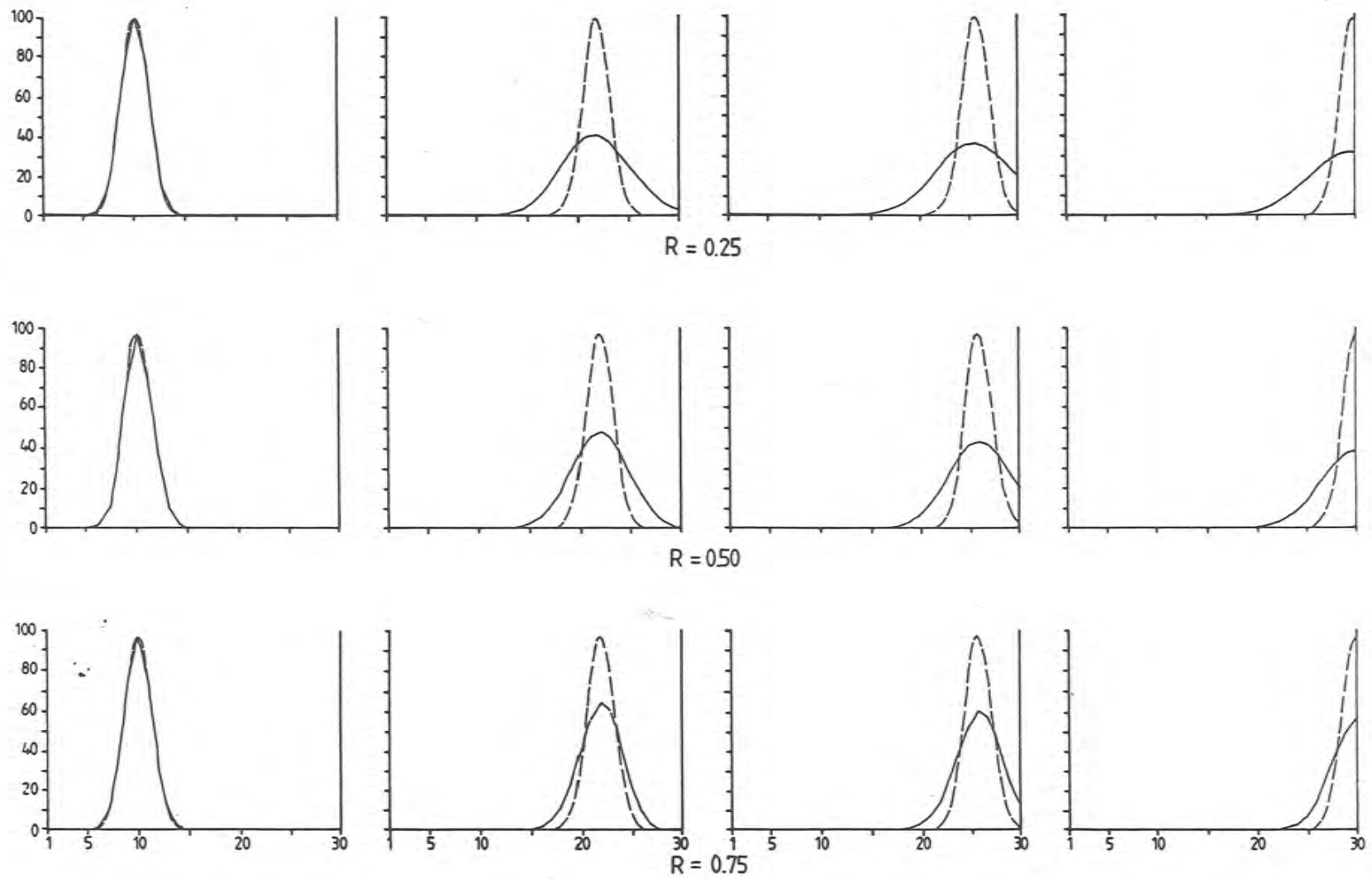


Figure 1b Finite differences Crank-Nicholson

28

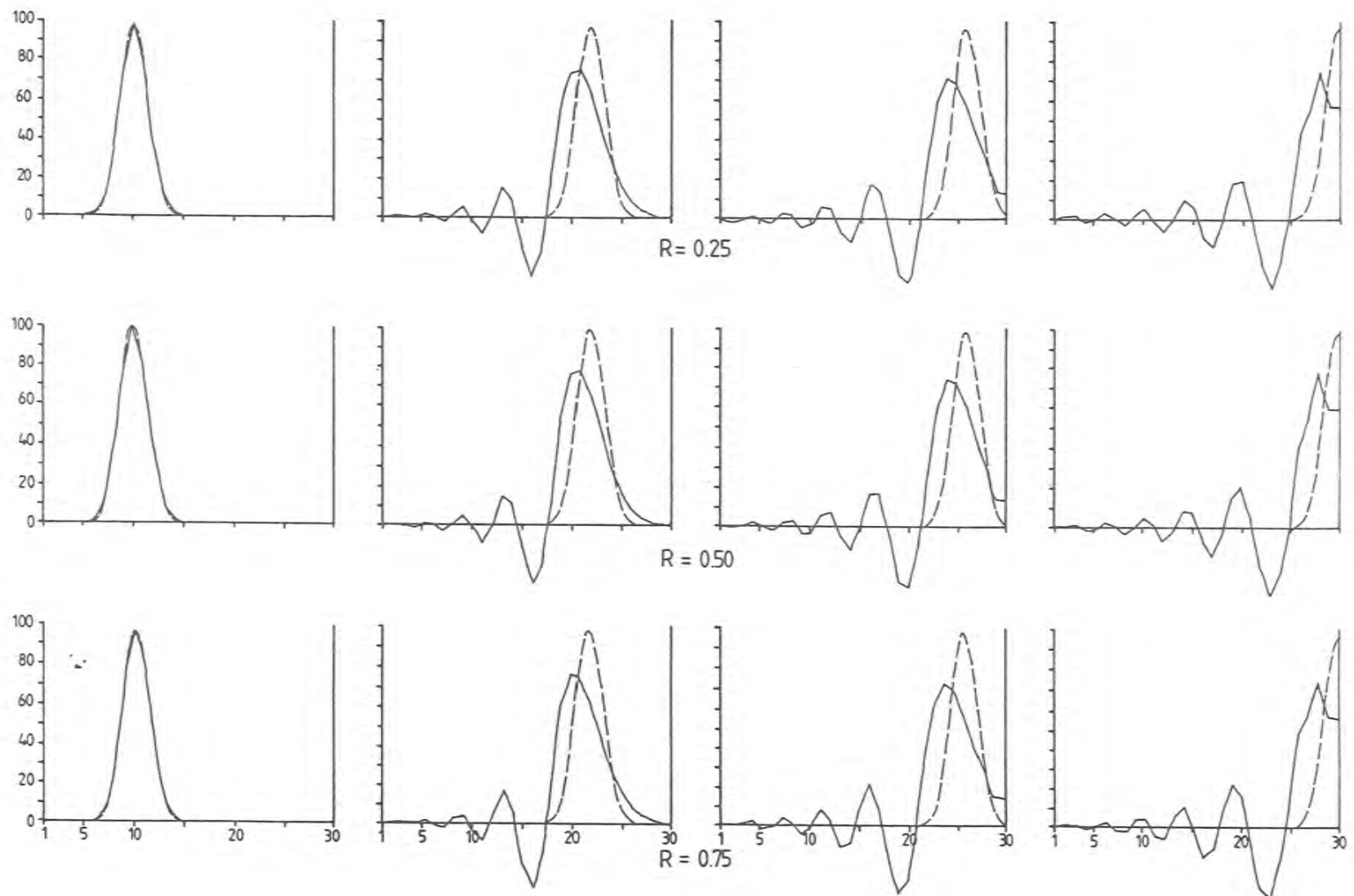


Figure 1c Finite differences Laasonen

29

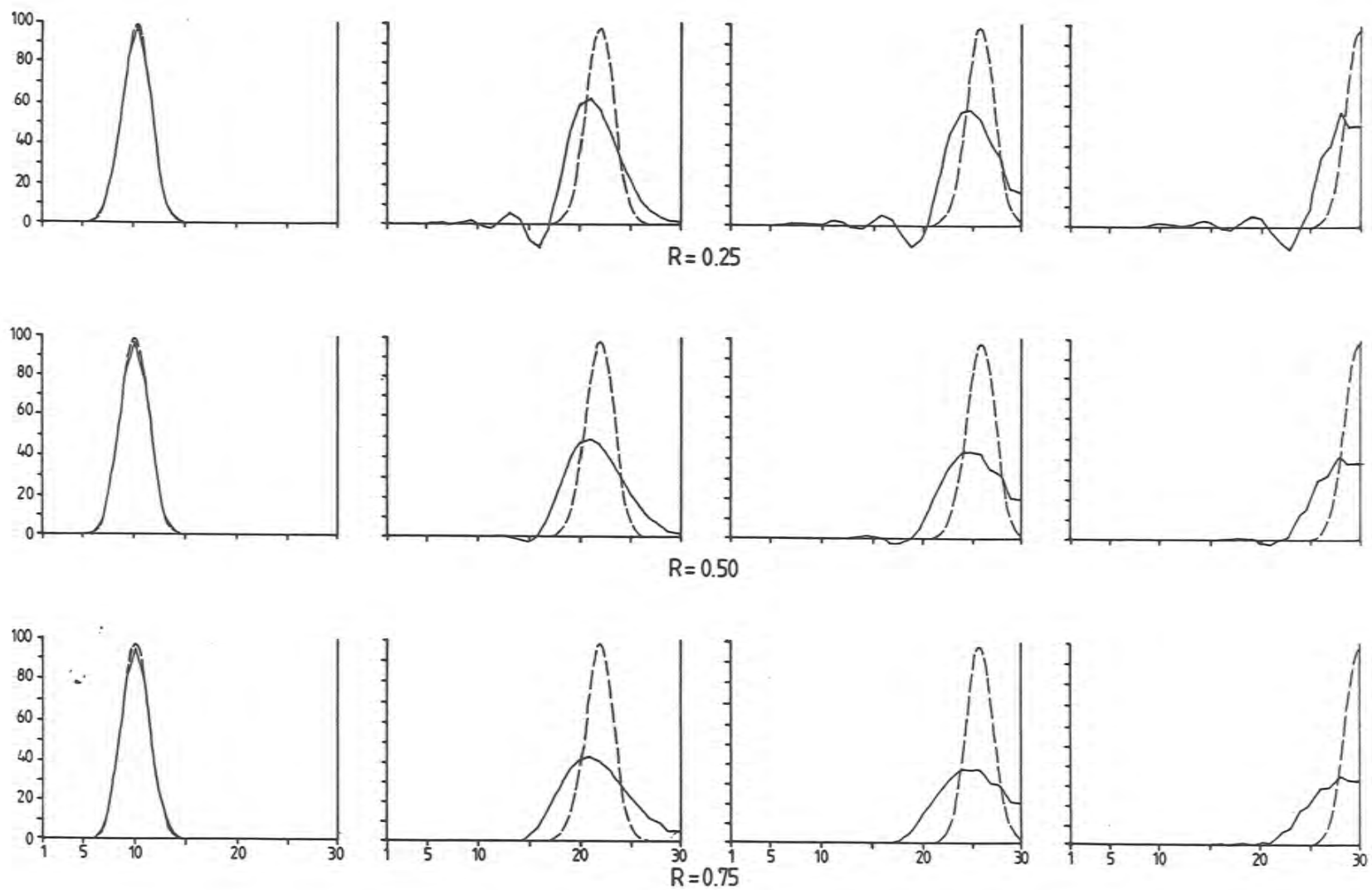


Figure 1d Finite differences Lax-Wendroff

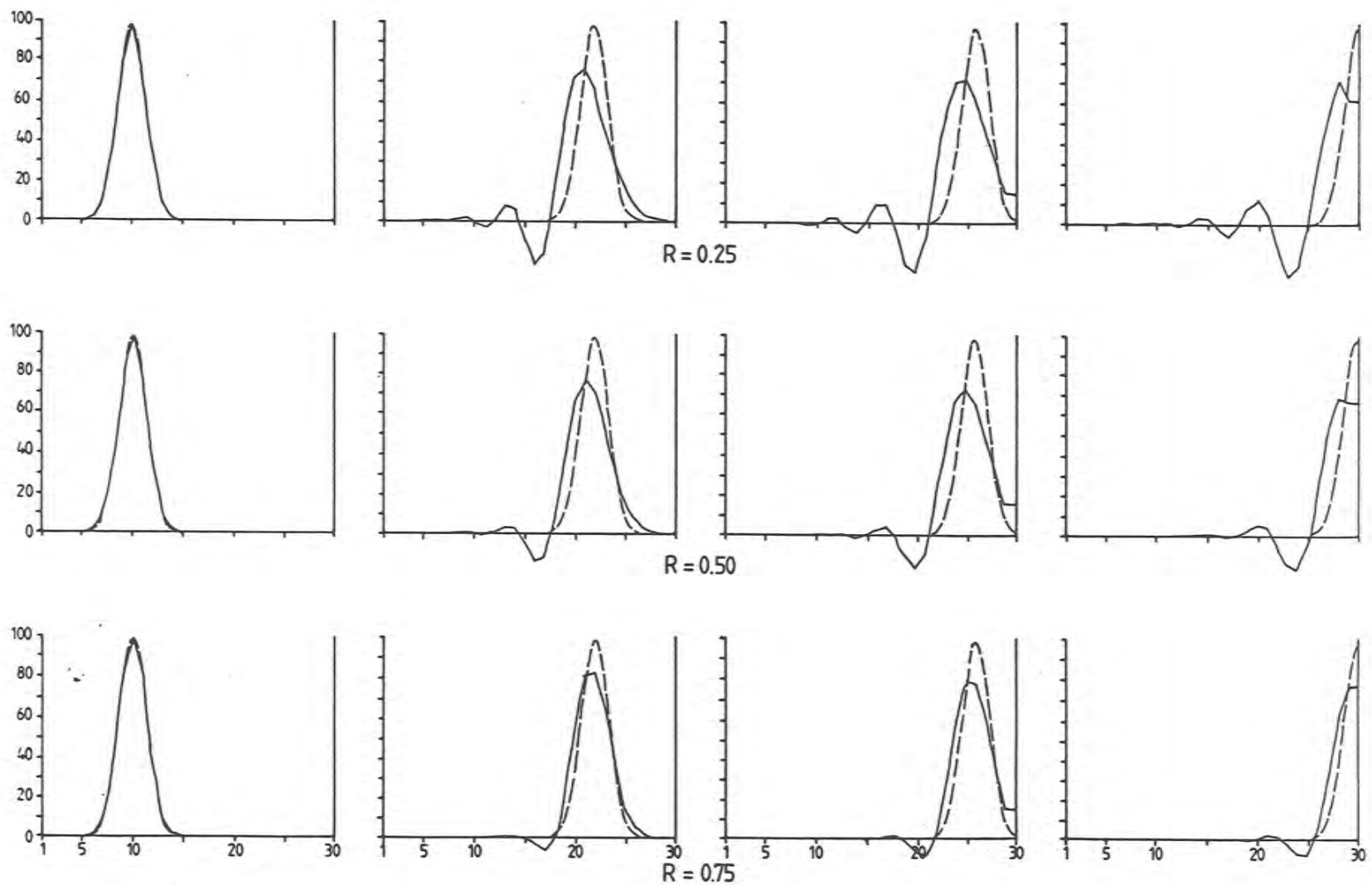


Figure 1e Finite differences leap frog

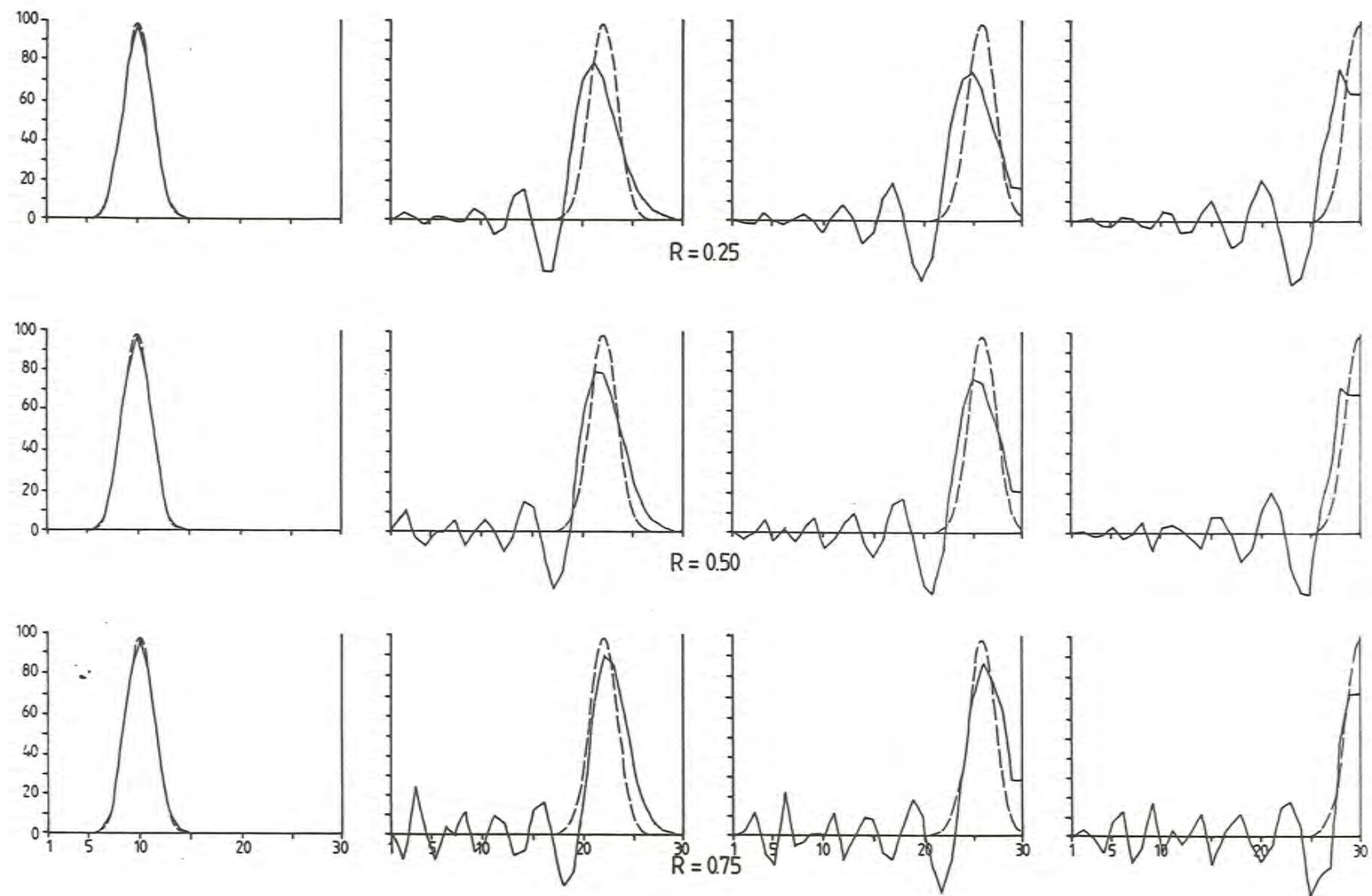


Figure 16 Linear finite element Crank-Nicholson

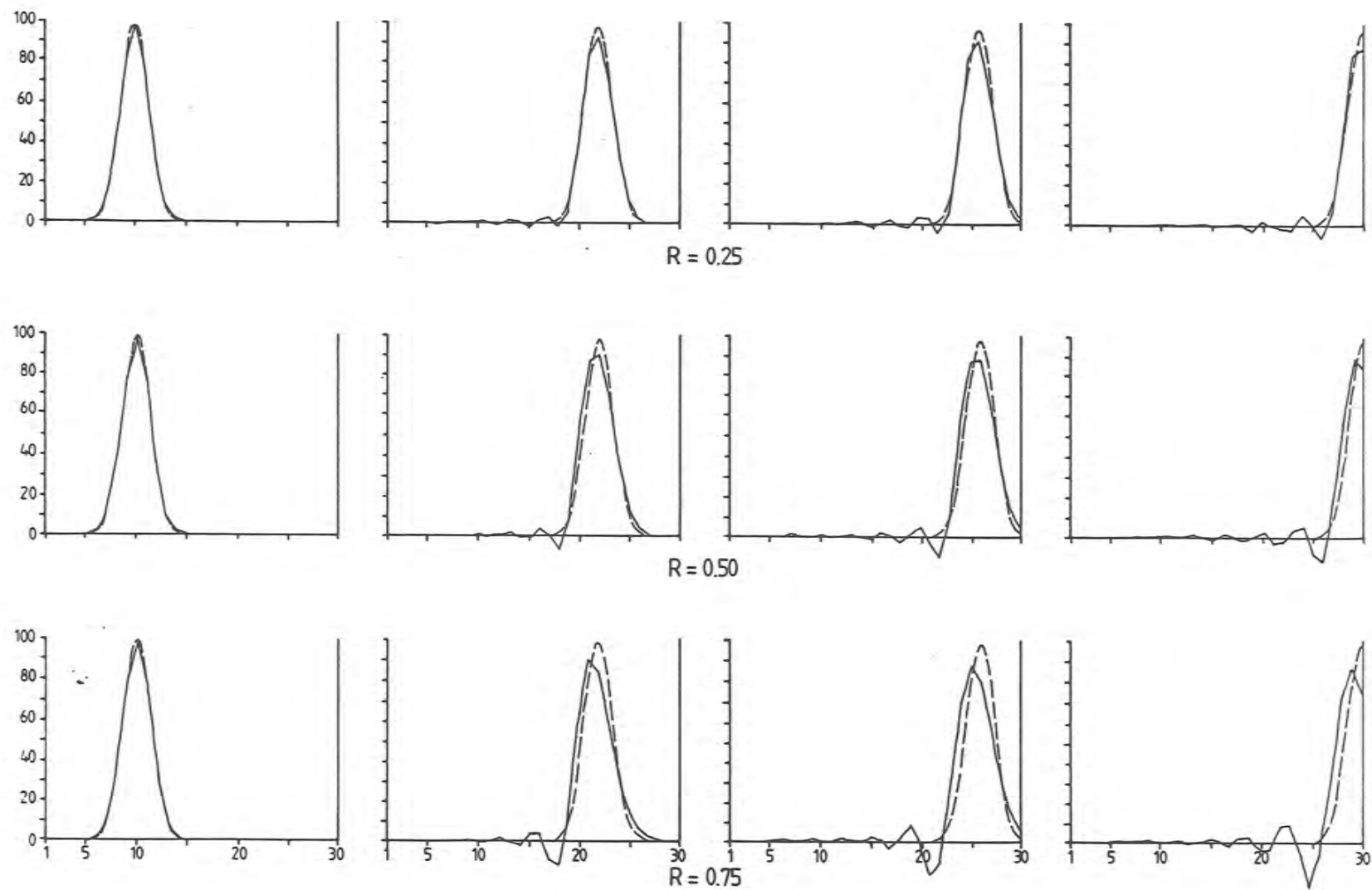


Figure 1g Pseudo-spectral leap frog

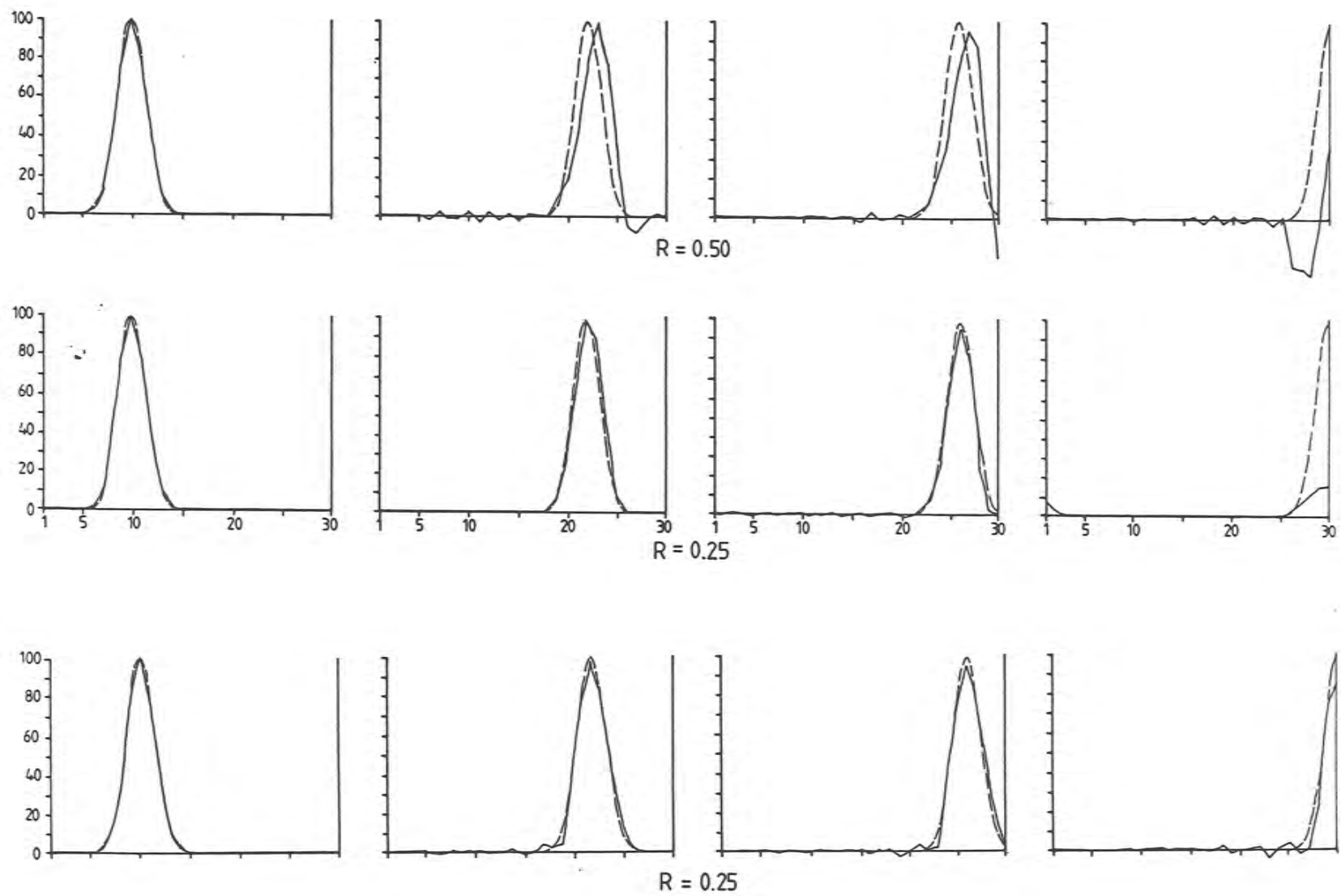


Figure 1h
Linear finite element
leap frog

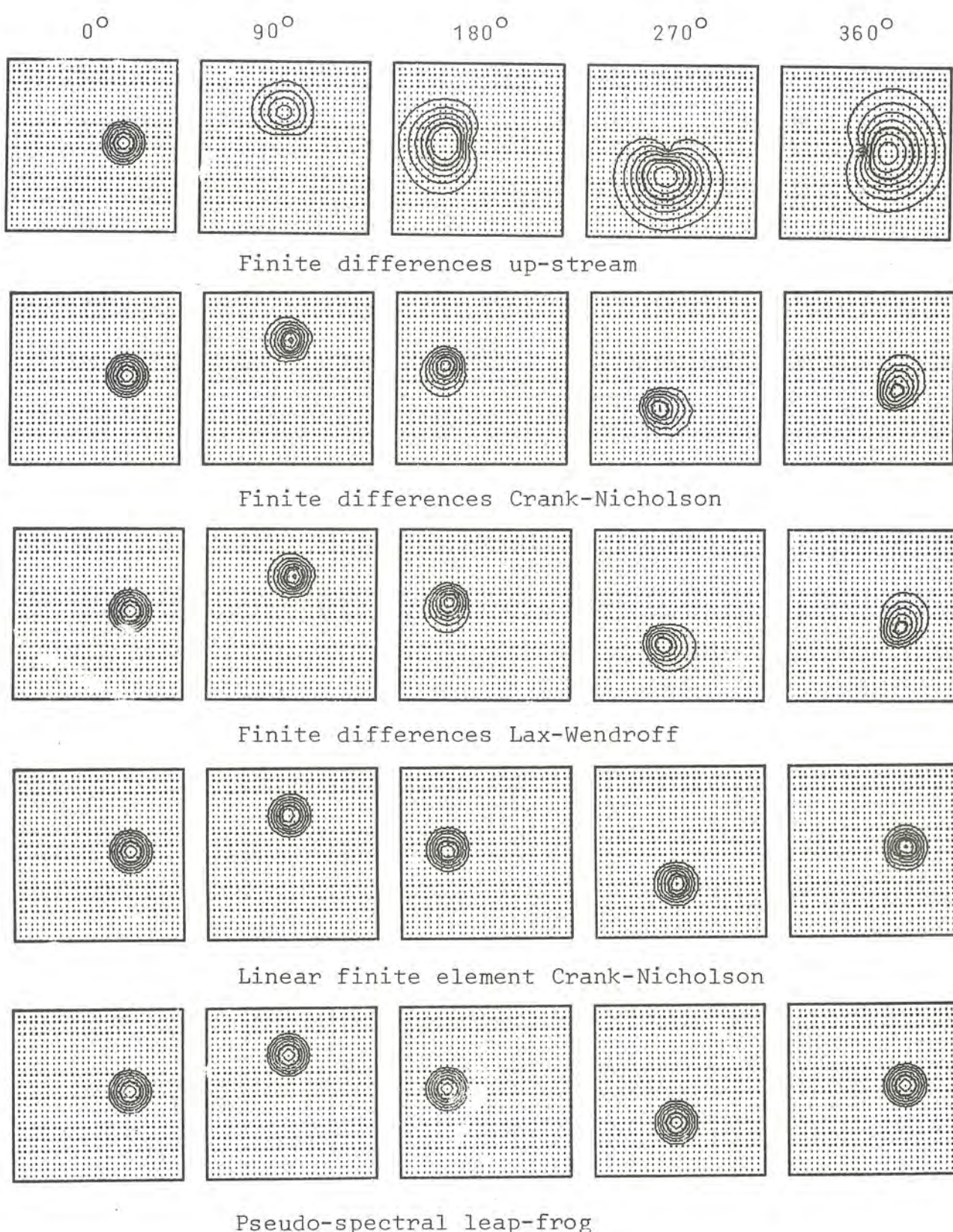
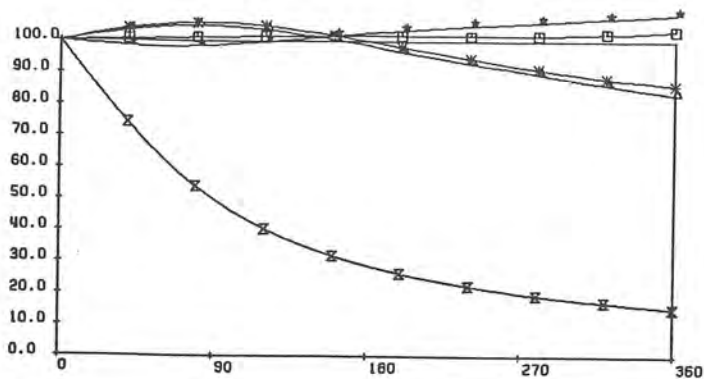
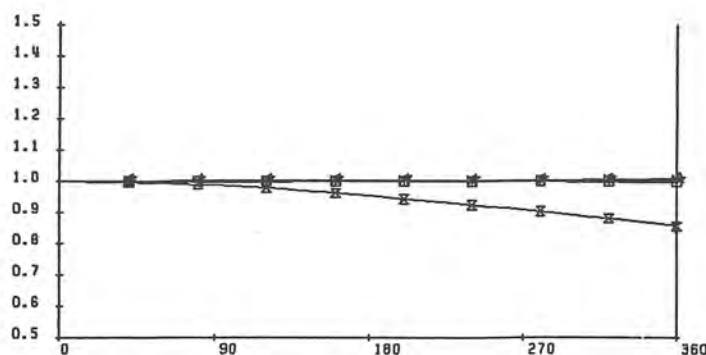


Figure 11a Angle of rotation

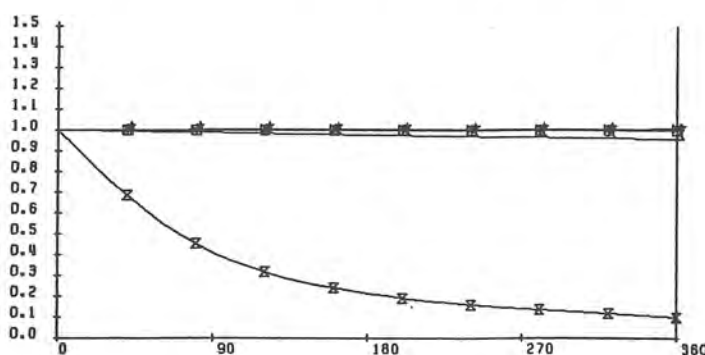
MAXIMAL AMPLITUDE



SUM OF AMPLITUDES



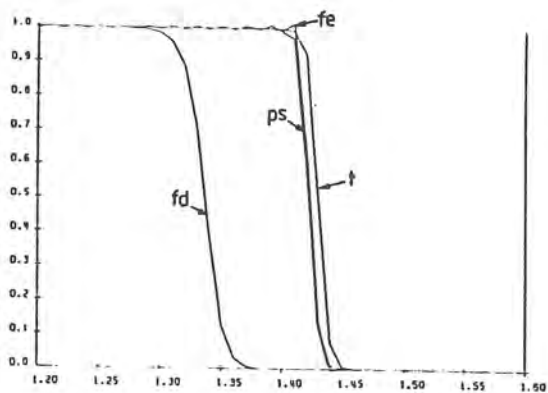
SUM OF AMPLITUDES SQUARES



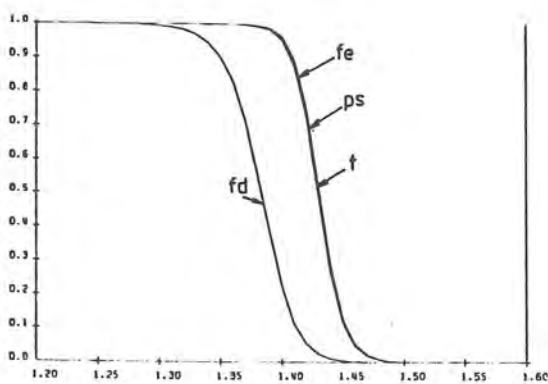
- ★ linear finite element Crank-Nicholson
- * finite differences Crank-Nicholson
- ✗ finite differences up-stream forwards
- ▲ finite differences Lax-Wendroff
- pseudo-spectral leap frog

Figure IIb

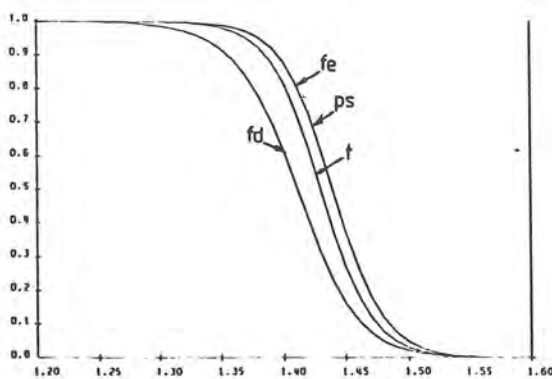
0.002



0.005



0.010



t true
ps pseudo-spectral
fe finite element
fd finite differences

Figure III

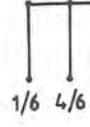
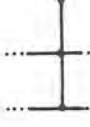
Table III

| K = 0.002 | | | | | K = 0.005 | | | | K = 0.001 | | | |
|-----------|-------|--------|-------|-------|-----------|-------|-------|-------|-----------|-------|-------|-------|
| x | t | ps | fe | fd | t | ps | fe | fd | t | ps | fe | fd |
| 1.37 | 1. | 1.007 | 0.999 | 0.007 | 0.998 | 0.998 | 0.999 | 0.717 | 0.963 | 0.970 | 0.972 | 0.839 |
| 1.38 | 1. | 0.997 | 1.001 | 0.001 | 0.993 | 0.994 | 0.996 | 0.560 | 0.924 | 0.952 | 0.954 | 0.779 |
| 1.39 | 1. | 1.008 | 0.999 | 0. | 0.982 | 0.984 | 0.988 | 0.382 | 0.881 | 0.923 | 0.925 | 0.704 |
| 1.40 | 0.999 | 0.991 | 0.995 | 0. | 0.953 | 0.957 | 0.964 | 0.224 | 0.818 | 0.879 | 0.880 | 0.615 |
| 1.41 | 0.993 | 0.969 | 1.014 | 0. | 0.881 | 0.891 | 0.898 | 0.116 | 0.731 | 0.814 | 0.815 | 0.515 |
| 1.42 | 0.924 | 0.610 | 0.655 | 0. | 0.731 | 0.750 | 0.752 | 0.055 | 0.622 | 0.727 | 0.726 | 0.412 |
| 1.43 | 0.5 | 0.128 | 0.139 | 0. | 0.5 | 0.525 | 0.523 | 0.025 | 0.5 | 0.617 | 0.616 | 0.315 |
| 1.44 | 0.076 | 0.010 | -0.03 | 0. | 0.269 | 0.289 | 0.288 | 0.011 | 0.378 | 0.494 | 0.493 | 0.230 |
| 1.45 | 0.007 | 0.007 | -0.01 | 0. | 0.119 | 0.131 | 0.129 | 0.005 | 0.269 | 0.372 | 0.371 | 0.161 |
| 1.46 | 0.001 | 0.003 | -0.01 | 0. | 0.047 | 0.053 | 0.050 | 0.002 | 0.182 | 0.265 | 0.264 | 0.110 |
| 1.47 | 0. | 0.001 | 0. | 0. | 0.018 | 0.020 | 0.018 | 0.001 | 0.119 | 0.179 | 0.179 | 0.073 |
| 1.48 | 0. | -0.001 | 0. | 0. | 0.007 | 0.008 | 0.006 | 0. | 0.076 | 0.117 | 0.117 | 0.048 |
| 1.49 | 0. | 0.001 | 0. | 0. | 0.002 | 0.003 | 0.002 | 0. | 0.047 | 0.075 | 0.074 | 0.031 |

t true
 ps pseudo-spectral fe finite element
 fd finite differences

Table IV

| Name and expression | Order of accuracy | Amplification factor | stability condition | Comput. model |
|---|--------------------------|---|---------------------------------------|---------------|
| finite differences forward or Euler (IVa) (NMC large scale boundary layer model) | $\Delta z^2, \Delta t$ | $g = 1+2S(\cos k\Delta z - 1) + iT \sin k\Delta z$ | $ T \leq 2S \leq 1$ | |
| finite differences trapezoidal (IVb) (Mahrt, 1971) | $\Delta z^2, \Delta t$ | $g = \frac{1+S(2 \cos k\Delta z - 1) + iT \sin k\Delta z}{1+S}$ | $S \leq 1$ and $T \leq 2S(S+1)$ | |
| finite differences (IVc) | $\Delta z^2, \Delta t$ | $g = \frac{1+2S \cos k\Delta z + iT \sin k\Delta z}{1+2S}$ | $T^2 \leq 2S(2S+1)$ | |
| finite differences Crank-Nicholson (IVd) | $\Delta z^2, \Delta t^2$ | $g = \frac{1+S(\cos k\Delta z - 1) + i \frac{T}{2} \sin k\Delta z}{1-S(\cos k\Delta z - 1) - i \frac{T}{2} \sin k\Delta z}$ | $\forall S$ $\forall T$ | |

| Name and expression | Order of accuracy | Amplification factor | Stability condition | Comput. model |
|---|-----------------------------|--|--|---|
| finite differences Laasonen (IVe) | $\Delta z^2, \Delta t$ | $g = \frac{1}{1-2S(\cos k\Delta z - 1) - iT \sin k\Delta z}$ | VS VT |  |
| finite differences Dufort-Frankel (IVf) | $\Delta z^2, \Delta t$ | g is solution of $g^2(1+2S) - 2g(2S \cos k\Delta z + iT \sin k\Delta z) - 1+2S = 0$ | $ T \leq 1$ |  |
| finite linear element Laasonen (IVg) | $\Delta z^2, \Delta t$ | $g = \frac{2+\cos k\Delta z}{2+\cos k\Delta z - 6S(\cos k\Delta z - 1) - iT \sin k\Delta z}$ | VS VT |  |
| pseudo-spectral Adams-Basforth (IVh) (Christensen and Prahm, 1976) | $\Delta z^\infty, \Delta t$ | g is solution of $g^2 - g(1 - \frac{3}{2} S(k\Delta z)^2 + i \frac{3}{2} T(k\Delta z)) - \frac{1}{2} S(k\Delta z)^2 + i \frac{1}{2} T(k\Delta z) = 0$ | $\pi^2 S \leq 1$ and $ T \pi \leq 2S$ |  |

| wave length $k\Delta z$ | $2\Delta z/\pi$ | $4\Delta z/\pi/2$ | $6\Delta z/\pi/3$ | $8\Delta z/\pi/4$ | |
|----------------------------|-----------------|-------------------|-------------------|-------------------|----------------|
| T = 0.25 | | | | | |
| S = 0.25 | ∞ | 2. | 0.943 1.183 | 0.903 1.073 | 0.891 1.040 |
| S = 0.50 | 0. | 0. | 1.124 4. | 1.107 1.561 | 1.025 1.248 |
| S = 0.75 | / | / | 0.314 -1.181 | 1.345 2.736 | 1.148 |
| T = 0.50 | | | | | |
| S = 0.25 | ∞ | 1. | 0.562 1. | 0.525 1. | 0.513 1. |
| S = 0.50 | 0. | 0. | 0.562 2. | 0.754 1.363 | 0.762 1.181 |
| S = 0.75 | / | / | 0.187 -1. | 0.843 2. | 0.889 1.433 |
| T = 0.75 | | | | | |
| S = 0.25 | ∞ | 0.667 | 0.168 0.834 | 0.029 0.909 | / |
| S = 0.50 | 0. | 0. | 0.233 1.333 | 0.363 1.165 | 0.400 1.092 |
| S = 0.75 | / | / | 0.056 -0.834 | 0.441 1.532 | 0.560 1.286 |

Table IVa - finite differences forward

| | | | | | |
|----------|-------|----|----------------|----------------|----------------|
| T = 0.25 | | | | | |
| S = 0.25 | 0.652 | 0. | 0.743 0.819 | 0.730 0.814 | 0.726 0.809 |
| S = 0.50 | 0.223 | 0. | 0.800 1.181 | 0.698 0.814 | 0.670 0.741 |
| S = 0.75 | 0.045 | 0. | 0.964 2. | 0.653 0.814 | 0.605 0.683 |
| T = 0.50 | | | | | |
| S = 0.25 | 0.652 | 0. | 0.530 0.749 | 0.501 0.780 | 0.491 0.790 |
| S = 0.50 | 0.223 | 0. | 0.610 1. | 0.583 0.780 | 0.571 0.726 |
| S = 0.75 | 0.045 | 0. | 0.617 1.410 | 0.576 0.780 | 0.549 0.671 |
| T = 0.75 | | | | | |
| S = 0.25 | 0.652 | 0. | 0.266 0.667 | 0.172 0.733 | 0.134 0.761 |
| S = 0.50 | 0.223 | 0. | 0.413 0.834 | 0.419 0.733 | 0.418 0.703 |
| S = 0.75 | 0.045 | 0. | 0.429 1.060 | 0.466 0.733 | 0.461 0.653 |

Table IVb - finite differences trapezoidal

ρ/K

$$\frac{d\rho}{dz} / \frac{dK}{dz}$$

/ unstable

| wave length $k\Delta z$ | $2\Delta z$ π | $4\Delta z$ $\pi/2$ | $6\Delta z$ $\pi/3$ | $8\Delta z$ $\pi/4$ |
|----------------------------|----------------------|------------------------|------------------------|------------------------|
| T = 0.25 | S = 0.25 | 0.445 | 0.608 | 0.611 |
| | | 0. | 0.624 | 0.655 |
| | S = 0.50 | ∞ | 0.537 | 0.506 |
| | S = 0.75 | 2. | 0.624 | 0.548 |
| T = 0.50 | S = 0.25 | 0.445 | 0.476 | 0.458 |
| | | 0. | 0.590 | 0.637 |
| | S = 0.50 | ∞ | 0.471 | 0.452 |
| | S = 0.75 | 1. | 0.590 | 0.537 |
| T = 0.75 | S = 0.25 | 0.445 | 0.296 | 0.229 |
| | | 0. | 0.546 | 0.610 |
| | S = 0.50 | ∞ | 0.381 | 0.368 |
| | S = 0.75 | 0.667 | 0.546 | 0.520 |

Table IVc - finite differences

| | | | | | |
|----------|----------|----------|-------|-------|-------|
| T = 0.25 | S = 0.25 | 0.445 | 0.814 | 0.906 | 0.944 |
| | | 0. | 0.674 | 0.837 | 0.903 |
| | S = 0.50 | ∞ | 0.869 | 0.920 | 0.949 |
| | S = 0.75 | -2. | 0.836 | 0.878 | 0.917 |
| T = 0.50 | S = 0.25 | 0.445 | 0.775 | 0.875 | 0.922 |
| | | 0. | 0.661 | 0.826 | 0.896 |
| | S = 0.50 | ∞ | 0.811 | 0.886 | 0.927 |
| | S = 0.75 | -1. | 0.801 | 0.864 | 0.910 |
| T = 0.75 | S = 0.25 | 0.445 | 0.717 | 0.827 | 0.888 |
| | | 0. | 0.641 | 0.810 | 0.884 |
| | S = 0.50 | ∞ | 0.734 | 0.834 | 0.892 |
| | S = 0.75 | -0.667 | 0.754 | 0.844 | 0.897 |

Table IVd - finite differences Crank-Nicholson

ρ/K

$\frac{dp}{dz} / \frac{dk}{dz}$ /unstable

| wave length $k\Delta z$ | $2\Delta z$ π | $4\Delta z$ $\pi/2$ | $6\Delta z$ $\pi/3$ | $8\Delta z$ $\pi/4$ |
|----------------------------|----------------------|------------------------|------------------------|------------------------|
| T = 0.25 | | | | |
| S = 0.25 | 0.281 | 0.680 | 0.868 | 0.962 |
| | 0. | 0.421 | 0.655 | 0.779 |
| S = 0.50 | 0.223 | 0.568 | 0.758 | 0.863 |
| | 0. | 0.317 | 0.548 | 0.692 |
| S = 0.75 | 0.187 | 0.498 | 0.690 | 0.803 |
| | 0. | 0.254 | 0.470 | 0.622 |
| T = 0.50 | | | | |
| S = 0.25 | 0.281 | 0.743 | 1.021 | 1.181 |
| | 0. | 0.410 | 0.637 | 0.762 |
| S = 0.50 | 0.223 | 0.586 | 0.812 | 0.950 |
| | 0. | 0.312 | 0.537 | 0.680 |
| S = 0.75 | 0.187 | 0.506 | 0.717 | 0.851 |
| | 0. | 0.251 | 0.463 | 0.613 |
| T = 0.75 | | | | |
| S = 0.25 | 0.281 | 0.838 | 1.250 | 1.515 |
| | 0. | 0.394 | 0.610 | 0.736 |
| S = 0.50 | 0.223 | 0.615 | 0.896 | 1.085 |
| | 0. | 0.305 | 0.520 | 0.661 |
| S = 0.75 | 0.187 | 0.518 | 0.759 | 0.925 |
| | 0. | 0.247 | 0.453 | 0.599 |

Table IVe - finite differences Laasonen

| | | | | |
|----------|----------|-------|-------|-------|
| T = 0.25 | | | | |
| S = 0.25 | 0.445 | 0.891 | 0.934 | 0.939 |
| | 0. | 0.746 | 0.924 | 0.966 |
| S = 0.50 | ∞ | 1.124 | 1.107 | 1.025 |
| | 2. | 4. | 1.561 | 1.248 |
| S = 0.75 | 0.217 | 0.315 | 0.672 | 0.990 |
| | 0. | 4. | 3.297 | 2.361 |
| T = 0.50 | | | | |
| S = 0.25 | 0.445 | 0.891 | 0.817 | 0.793 |
| | 0. | 0.784 | 0.946 | 0.975 |
| S = 0.50 | ∞ | 0.562 | 0.754 | 0.762 |
| | 1. | 2. | 1.363 | 1.181 |
| S = 0.75 | 0.217 | 0.201 | 0.409 | 0.580 |
| | 0. | 2. | 1.763 | 1.521 |
| T = 0.75 | | | | |
| S = 0.25 | 0.445 | 0.891 | 0.574 | 0.506 |
| | 0. | 0.889 | 0.980 | 0.989 |
| S = 0.50 | ∞ | 0.233 | 0.363 | 0.400 |
| | 0.567 | 1.333 | 1.165 | 1.092 |
| S = 0.75 | 0.217 | 0.095 | 0.189 | 0.266 |
| | 0. | 1.333 | 1.258 | 1.190 |

Table IVf - finite differences Dufort-Frankell

p/K

$$\frac{dp}{dz} / \frac{dk}{dz}$$

/unstable

| wave length $k\Delta z$ | $2\Delta z$ π | $4\Delta z$ $\pi/2$ | $6\Delta z$ $\pi/3$ | $8\Delta z$ $\pi/4$ |
|----------------------------|----------------------|------------------------|------------------------|------------------------|
| T = 0.25 | | | | |
| S = 0.25 | 0.562 | 0.944 | 1.028 | 1.066 |
| S = 0.50 | 0.394 | 0.538 | 0.753 | 0.850 |
| S = 0.75 | 0.311 | 0.379 | 0.615 | 0.748 |
| | 0. | 0.640 | 0.792 | 0.876 |
| | | 0.293 | 0.519 | 0.667 |
| T = 0.50 | | | | |
| S = 0.25 | 0.562 | 1.044 | 1.227 | 1.324 |
| S = 0.50 | 0.394 | 0.516 | 0.726 | 0.828 |
| S = 0.75 | 0.311 | 0.778 | 0.949 | 1.047 |
| | 0. | 0.371 | 0.600 | 0.732 |
| | | 0.651 | 0.824 | 0.930 |
| | | 0.289 | 0.510 | 0.656 |
| T = 0.75 | | | | |
| S = 0.25 | 0.562 | 1.188 | 1.517 | 1.713 |
| S = 0.50 | 0.394 | 0.485 | 0.688 | 0.795 |
| S = 0.75 | 0.311 | 0.817 | 1.051 | 1.133 |
| | 0. | 0.359 | 0.577 | 0.709 |
| | | 0.667 | 0.875 | 1.014 |
| | | 0.283 | 0.496 | 0.639 |

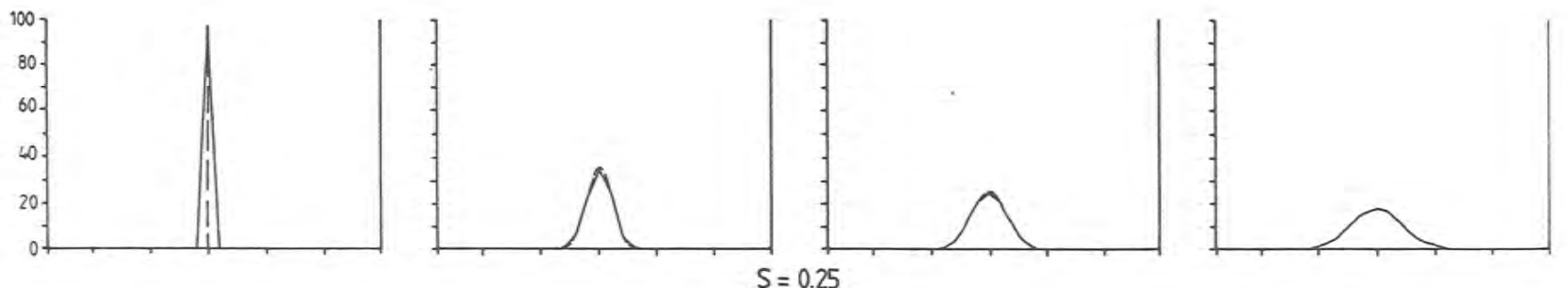
ρ/K

$\frac{d\rho}{dz}/\frac{dK}{dz}$

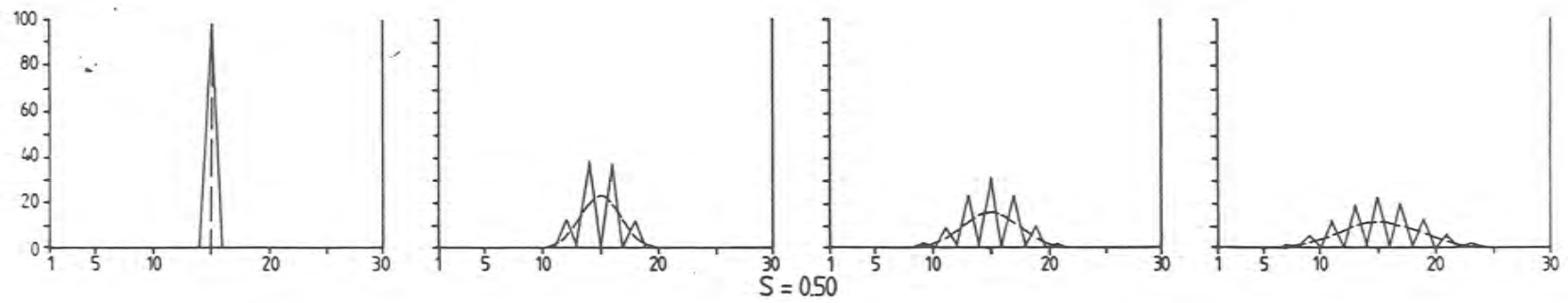
/ unstable

Table IVg - linear finite element Laasonen

Figure IVa Finite differences forward



$S = 0.25$



$S = 0.50$

Figure IVb Finite differences trapezoidal

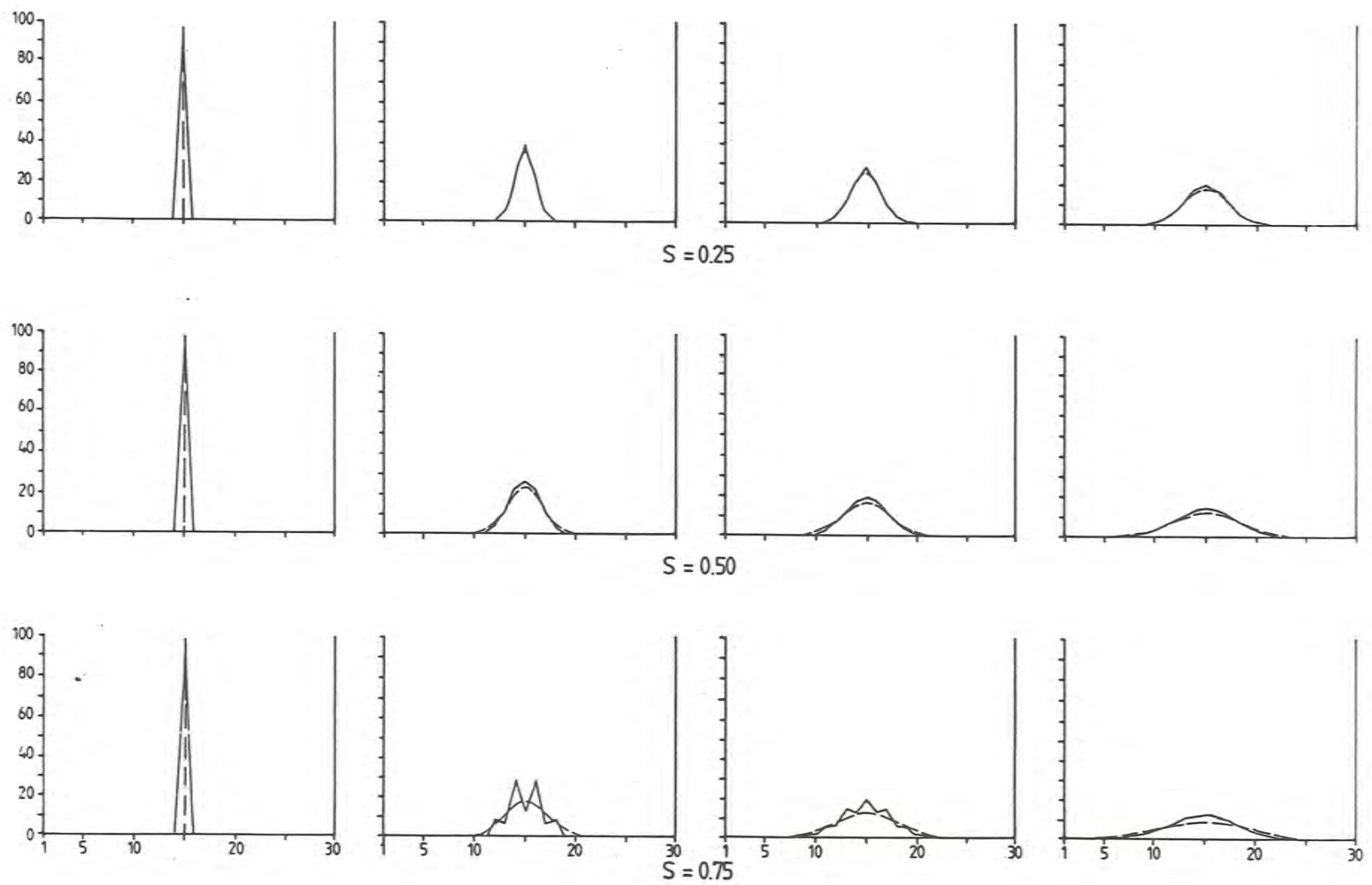


Figure IVc Finite differences

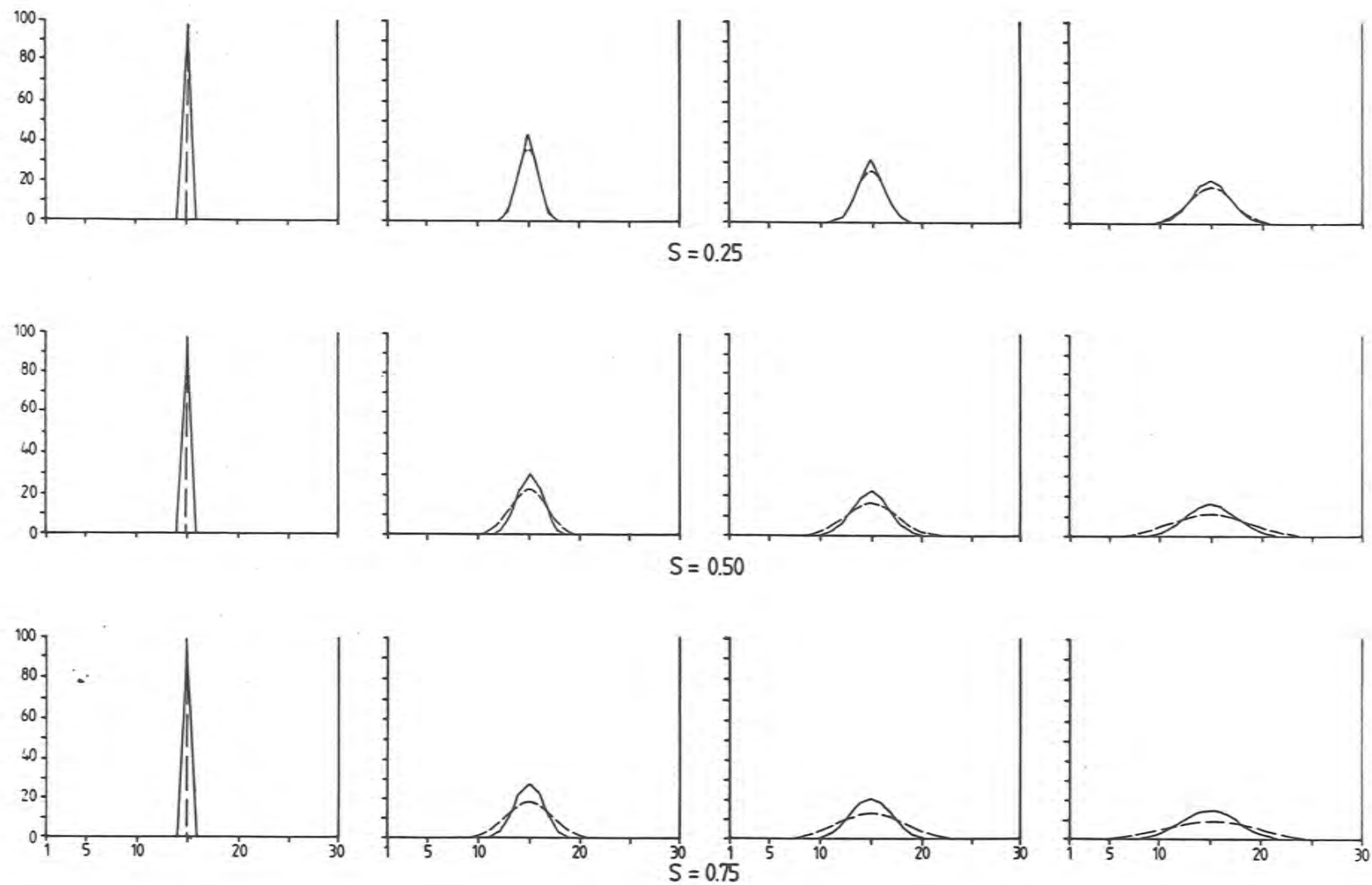


Figure IVd Finite differences Crank-Nicholson

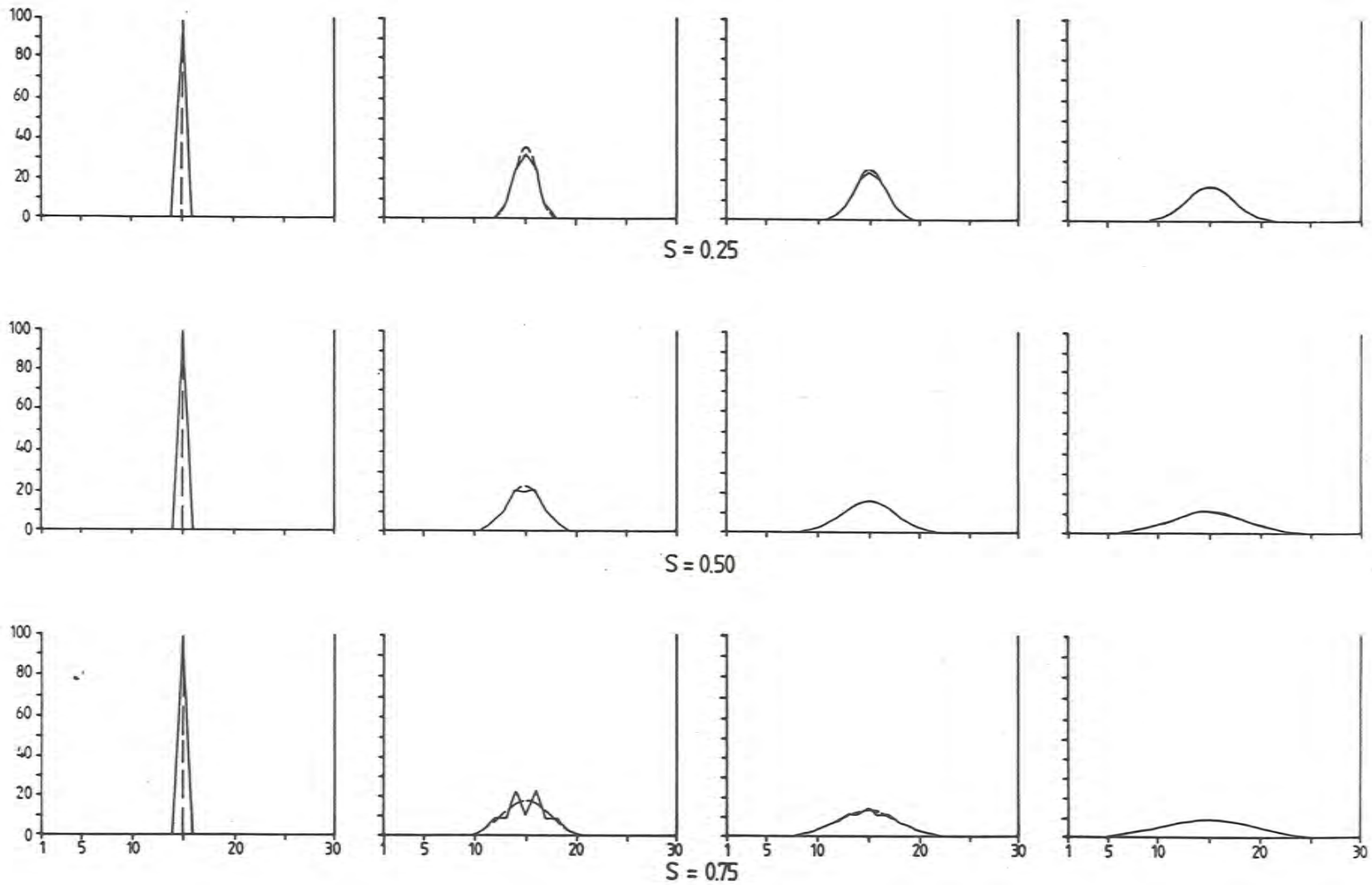


Figure IVE Finite differences Laasonen

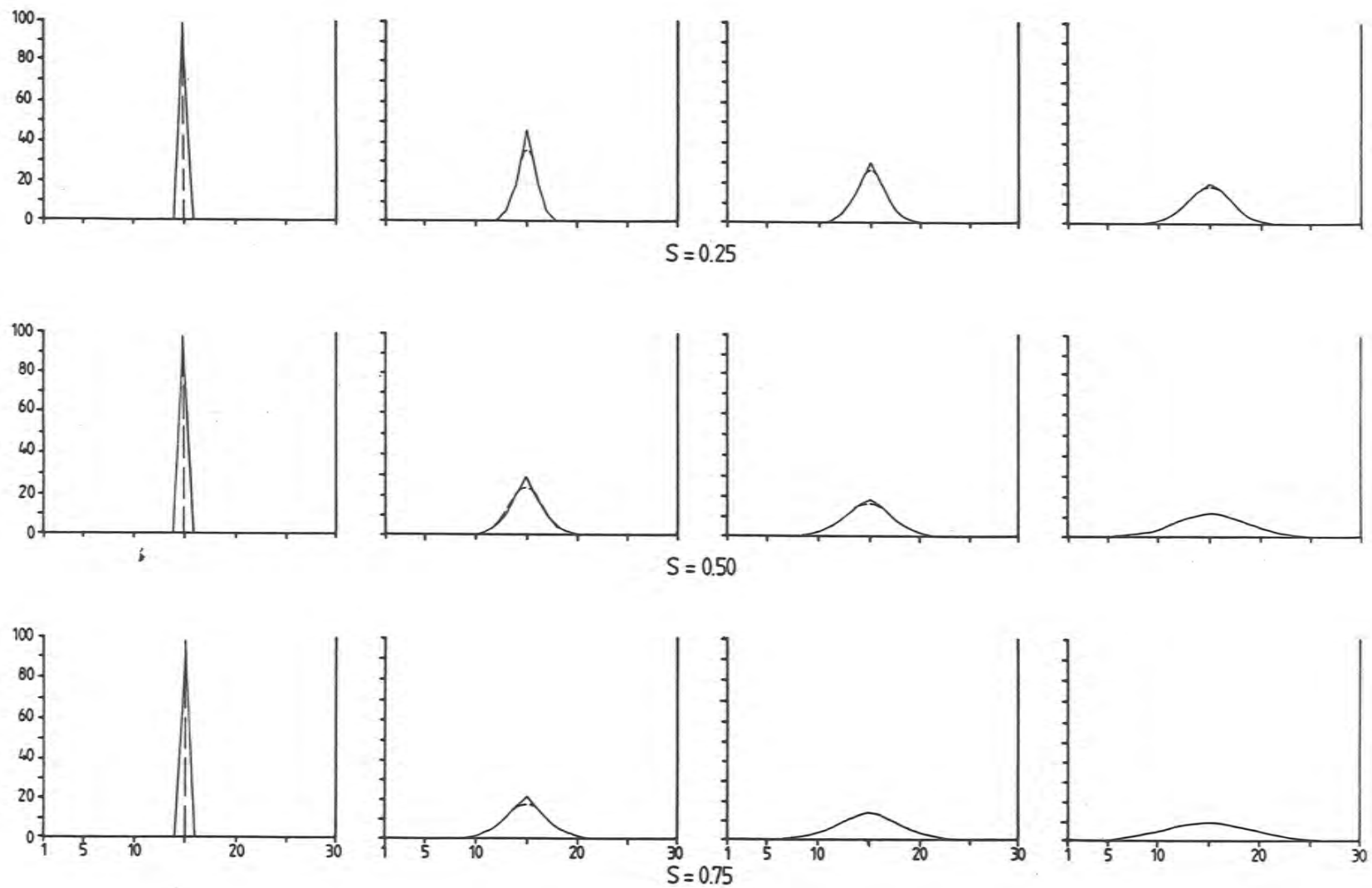


Figure IV.6 Finite differences Dufort-Frankel

49

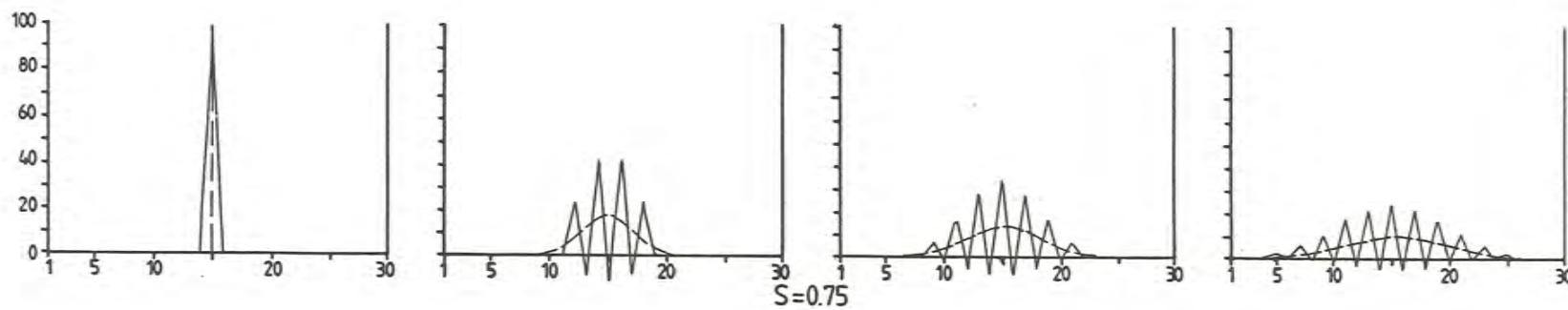
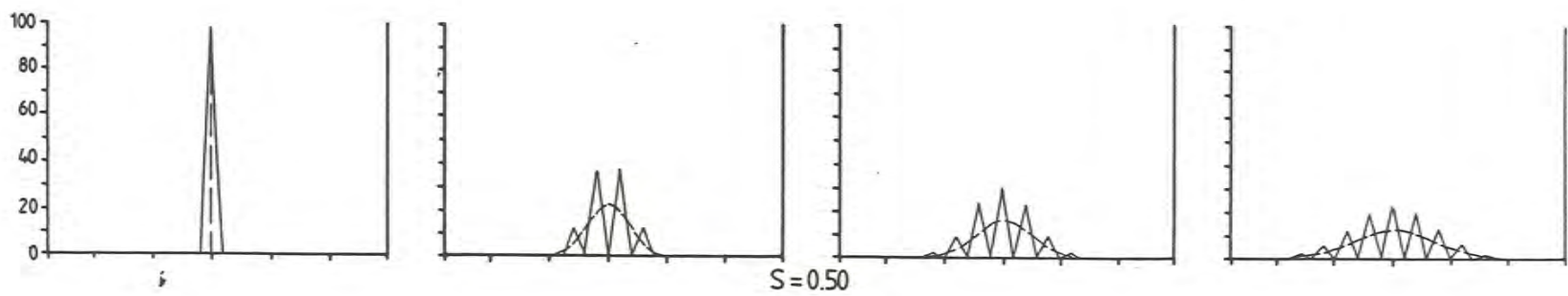
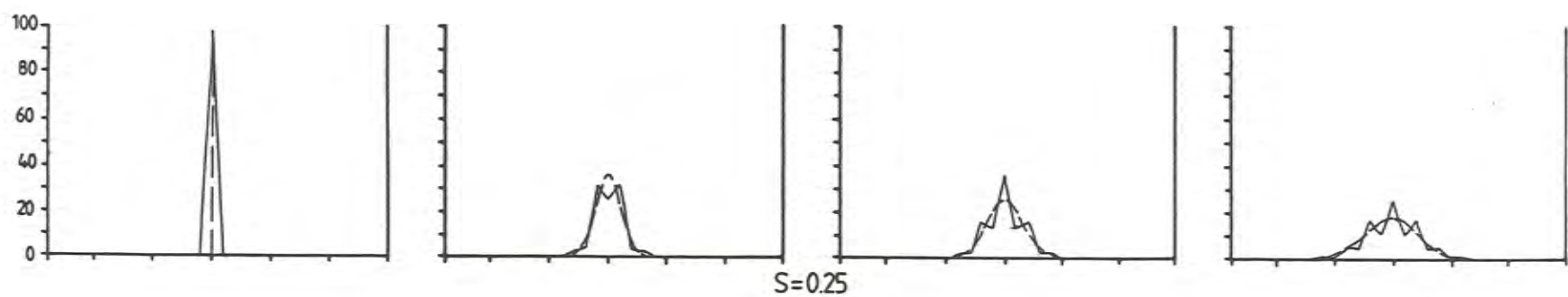


Figure IVg Linear finite element Laasonen

50

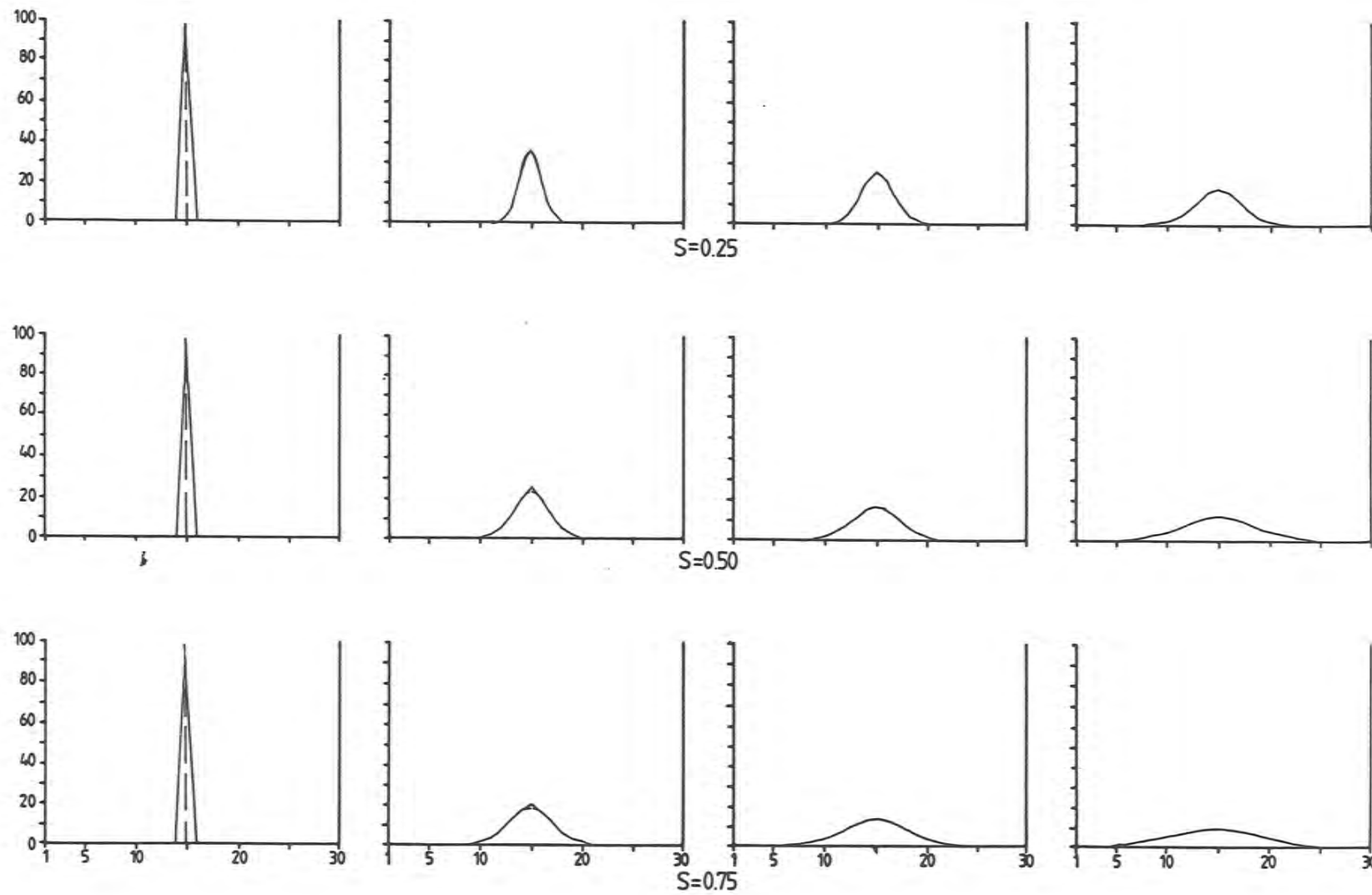


Figure IVh Pseudo-spectral Adams-Basforth

51

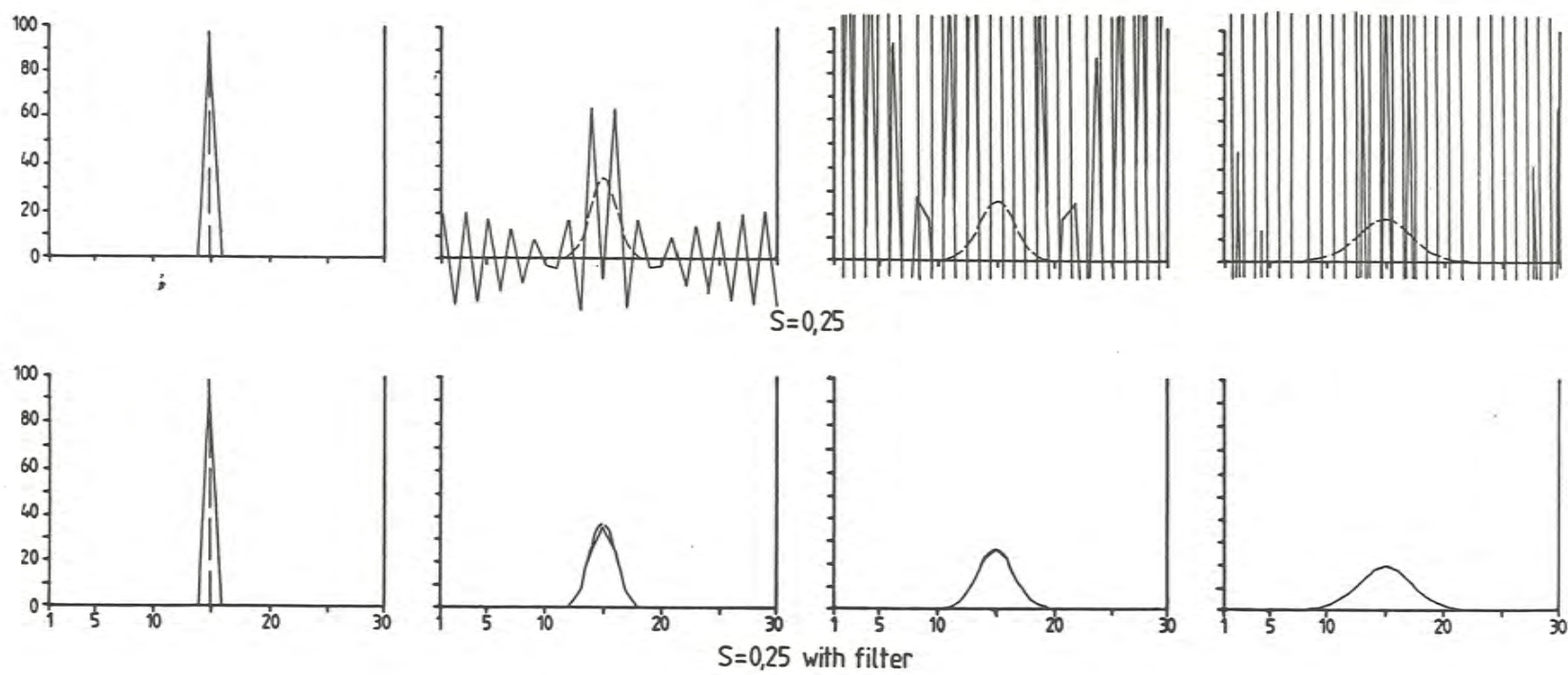
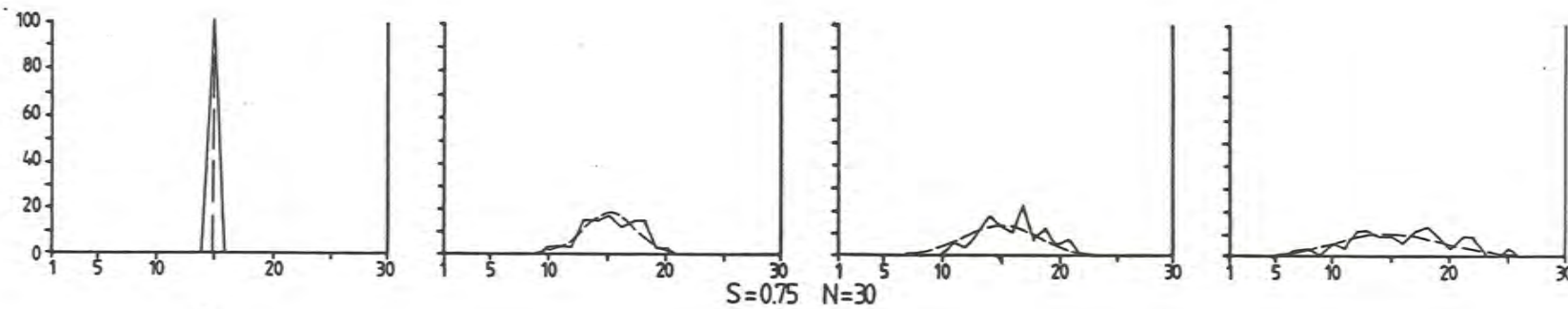
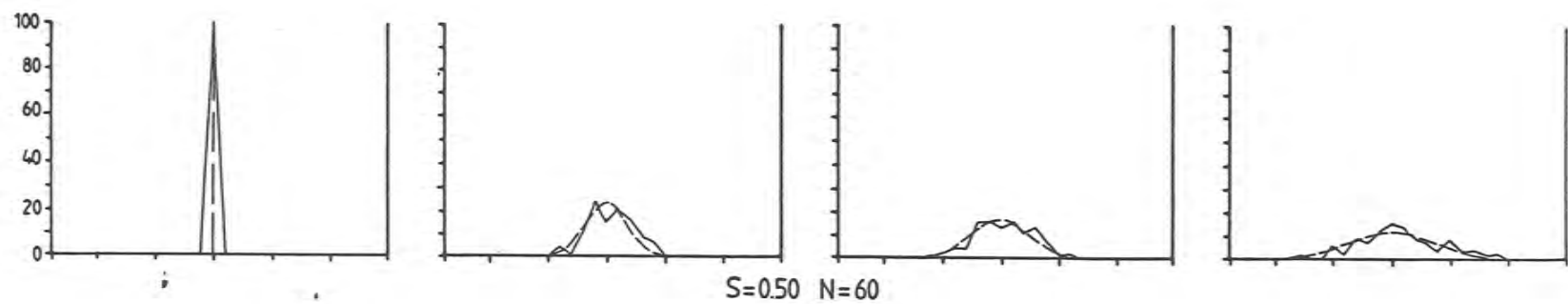
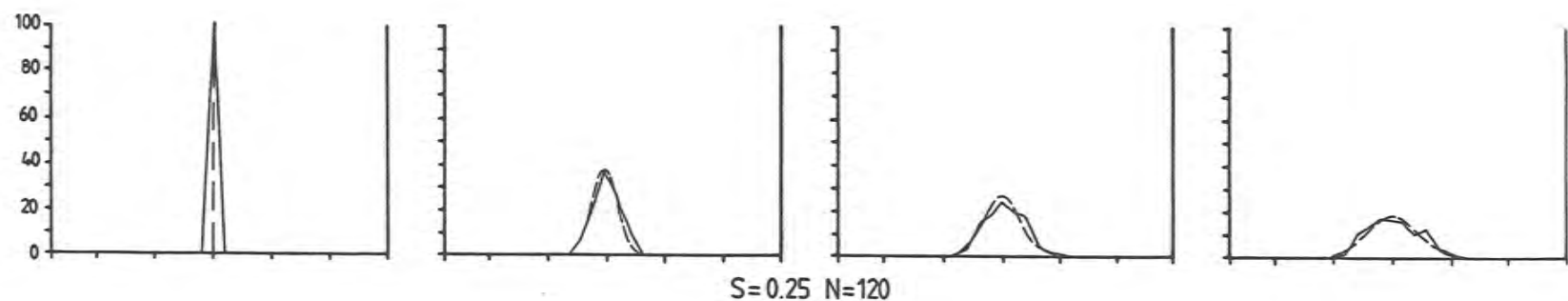


Figure V Random walk

52



| Wave length | $2\Delta s$ | $4\Delta s$ | $6\Delta s$ | $8\Delta s$ |
|-------------|-------------|-------------|-------------|-------------|
| $v = 0.005$ | 0.990 | 0.995 | 0.997 | 0.998 |
| $v = 0.05$ | 0.9 | 0.95 | 0.975 | 0.985 |
| $v = 0.5$ | 0. | 0.5 | 0.75 | 0.853 |
| $v = 1$ | -1. | 0. | 0.5 | 0.707 |

Table VIa Asselin filter

| | | | | |
|------------|----|-------|-------|-------|
| $v = 0.01$ | 0. | 0.990 | 0.996 | 0.998 |
| $v = 0.05$ | 0. | 0.952 | 0.983 | 0.991 |
| $v = 0.1$ | 0. | 0.909 | 0.967 | 0.983 |
| $v = 0.25$ | 0. | 0.8 | 0.923 | 0.959 |
| $v = 1.$ | 0. | 0.5 | 0.75 | 0.853 |

Table VIb Long filter

REFERENCES

- Arakawa, A., 1976: Numerical methods used in atmospheric models. GARP Publications series No 17, 1.
- Asselin, R., 1972: Frequency filter for time integrations. Mon. Wea. Rev., 100, pp 487-490.
- Christensen, O. and Prahm, L.P., 1976: A pseudo-spectral model for dispersion of atmospheric pollutants. Journal of Applied Meteor., 15, 1284-1294.
- Csanady, G.T., 1973: Turbulent diffusion in the environment. D. Reidel Publ. comp.
- Cullen, J.P., 1979: Numerical methods used in atmospheric models. GARP Publications series No 17, 2.
- Gadd, A.J., 1974: Fourth order advection schemes for the 10 level model. Meteorological Office Tech Note 45.
- Gazdag, J., 1973: Numerical convective schemes based on accurate computation of space derivatives. Journal of Computational Physics, 13, pp 100-113.
- Holton, J.R., 1979: An introduction to dynamic meteorology. Academic Press, New York.
- Johnson, C., 1980: Numerisk lösning av partiella differentialekvationer med finite element metoden. ISBN 91-44-16351-7. University of Lund, Sweden.
- Long, P.E., 1975: Dissipation, dispersion and difference schemes. NOAA Techn. Memo. NWS TDL-56.
- Long, P.E., Shaffer, W.A., Kemper, J.E. and Hicks, F.J., 1977: The state of the TDL's boundary layer model. NOAA Techn. Memo. NWS TDL 66.
- Mahrt, L., 1971: A numerical study of advective effects on boundary layer flow at low latitudes. Report, ESSA Grant E. 230-68G, University of Wisconsin.
- Merilees, P.E. and Orszag, I.A., 1979: Numerical methods used in atmospheric models. GARP Publications series No 17, 2.

Nappo, C.J., 1972: Status report on the ATDL planetary boundary layer numerical modelling program. NOAA, Oak Ridge, Tennessee.

Tag, P.M., 1969: Surface temperature in an urban environment. Report No 15, NSF Grant-GA-3956, Pennsylvania State University.

Tennekes, H. and Lumley, J.L., 1972: A first course in turbulence. MIT Press, Cambridge, Massachusetts.

SMHI Rapporter, METEOROLOGI OCH KLIMATOLOGI (RMK)

- Nr 1 Thompson, T, Udin, I and Omstedt, A
Sea surface temperatures in waters surrounding Sweden. (1974)
- Nr 2 Bodin, S
Development on an unsteady atmospheric boundary layer model. (1974)
- Nr 3 Moen, L
A multi-level quasi-geostrophic model for short range weather predictions. (1975)
- Nr 4 Holmström, I
Optimization of atmospheric models. (1976)
- Nr 5 Collins, W G,
A parameterization model for calculation of vertical fluxes of momentum due to terrain induced gravity waves. (1976)
- Nr 6 Nyberg, A
On transport of sulphur over the North Atlantic. (1976)
- Nr 7 Lundqvist, J-E and Udin, I
Ice accretion on ships with special emphasis on Baltic conditions. (1977)
- Nr 8 Eriksson, B
Den dagliga och årliga variationen av temperatur, fuktighet och vindhastighet vid några orter i Sverige. (1977)
- Nr 9 Holmström, I and Stokes, J
Statistical forecasting of sea level changes in the Baltic. (1978)
- Nr 10 Omstedt, A and Sahlberg, J
Some results from a joint Swedish-Finnish Sea Ice Experiment, March, 1977. (1978)
- Nr 11 Haag, T
Byggnadsindustrins väderberoende, seminarieuppsats i företagsekonomi, B-nivå. (1978)
- Nr 12 Eriksson, B
Vegetationsperioden i Sverige beräknad från temperaturobservationer. (1978)
- Nr 13 Bodin, S
En numerisk prognosmodell för det atmosfäriska gränsskiktet grundad på den turbulenta energiekvationen.
- Nr 14 Eriksson, B
Temperaturfluktuationer under senaste 100 åren. (1979)
- Nr 15 Udin, I och Mattisson, I
Havsis- och snöinformation ur datorbearbetade satellitdata - en modellstudie. (1979)
- Nr 16 Eriksson, B
Statistisk analys av nederbörsdata. Del I. Arealnederbörd(1979)
- Nr 17 Eriksson, B
Statistisk analys av nederbörsdata. Del II. Frekvensanalys av månadsnederbörd. (1980)
- Nr 18 Eriksson, B
Årsmedelvärden (1931-60) av nederbörd, avdunstning och avrinning. (1980)
- Nr 19 Omstedt, A
A sensitivity analysis of steady, free floating ice. (1980)

- Nr 20 Persson, C och Omstedt, G
En modell för beräkning av luftföroreningars spridning och deposition på mesoskala (1980)
- Nr 21 Jansson, D
Studier av temperaturinversioner och vertikal vindskjuvning vid Sundsvall-Härnösands flygplats (1980)
- Nr 22 Sahlberg, J and Törnevik, H
A study of large scale cooling in the Bay of Bothnia (1980)
- Nr 23 Ericson, K and Hårsman, P-O
Boundary layer measurements at Klockrike. Oct 1977 (1980)
- Nr 24 Bringfelt, B
A comparison of forest evapotranspiration determined by some independent methods (1980)
- Nr 25 Bodin, S and Fredriksson, U
Uncertainty in wind forecasting for wind power networks (1980)
- Nr 26 Eriksson, B
Graddagsstatistik för Sverige (1980)
- Nr 27 Eriksson, B
Statistisk analys av nederbördssdata. Del III 200-åriga nederbördsserier. (1981)
- Nr 28 Eriksson, B
Den "potentiella" evapotranspirationen i Sverige (1981)
- Nr 29 Pershagen, H
Maximisnödjup i Sverige (perioden 1905-70) (1981)
- Nr 30 Lönnqvist, O
Nederbördssstatistik med praktiska tillämpningar
(Precipitation statistics with practical applications)
(1981)
- Nr 31 Melgarejo, J W
Similarity theory and resistance laws for the atmospheric boundary layer (1981)
- Nr 32 Liljas, E
Analys av moln och nederbörd genom automatisk klassning av AVHRR data (1981)
- Nr 33 Ericson, K
Atmospheric Boundary Layer Field Experiment in Sweden 1980, GOTEX II, part I (1982)
- Nr 34 Schoeffler, P
Dissipation, dispersion and stability of numerical schemes for advection and diffusion (1982)



SWEDISH METEOROLOGICAL AND HYDROLOGICAL INSTITUTE
Box 923 S-601 19 Norrköping, Sweden. Phone +46 11 10 80 00. Telex 644 00 smhi s

ISSN 0347-2116